

Solvable model for a dynamical quantum phase transition from fast to slow scrambling

Sumilan Banerjee^{1,2} and Ehud Altman^{1,3}

¹*Department of Condensed Matter Physics, Weizmann Institute of Science, Rehovot 76100, Israel*

²*Department of Physics, Indian Institute of Science, Bangalore 560012, India*

³*Department of Physics, University of California, Berkeley, California 94720, USA*

(Received 7 November 2016; published 19 April 2017)

We propose an extension of the Sachdev-Ye-Kitaev (SYK) model that exhibits a quantum phase transition from the previously identified non-Fermi-liquid fixed point to a Fermi-liquid-like state, while still allowing an exact solution in a suitable large- N limit. The extended model involves coupling the interacting N -site SYK model to a new set of pN peripheral sites with only quadratic hopping terms between them. The conformal fixed point of the SYK model remains a stable low-energy phase below a critical ratio of peripheral sites $p < p_c(n)$ that depends on the fermion filling n . The scrambling dynamics throughout the non-Fermi-liquid (NFL) phase is characterized by a universal Lyapunov exponent $\lambda_L \rightarrow 2\pi T$ in the low-temperature limit; however, the temperature scale marking the crossover to the conformal regime vanishes continuously at the critical point p_c . The residual entropy at $T \rightarrow 0$, nonzero in the NFL, also vanishes continuously at the critical point. For $p > p_c$ the quadratic sites effectively screen the SYK dynamics, leading to a quadratic fixed point in the low-temperature and low-frequency limit. The interactions have a perturbative effect in this regime leading to scrambling with Lyapunov exponent $\lambda_L \propto T^2$.

DOI: [10.1103/PhysRevB.95.134302](https://doi.org/10.1103/PhysRevB.95.134302)

I. INTRODUCTION

Kitaev [1] recently gave an intriguing new interpretation to a model of many fermions with all-to-all interactions, introduced originally by Sachdev and Ye as a solvable example of a non-Fermi liquid [2]. The work of Sachdev and Ye followed by Parcollet and Georges [3] investigated the saddle-point solution, which is exact in the thermodynamic (large- N) limit and realizes a nontrivial conformal fixed point. The more recent work on this problem, initiated by Kitaev [1,4–6], used a simplified version henceforth called the Sachdev-Ye-Kitaev (SYK) model and focused on the dynamics leading to ergodicity, chaos, and scrambling of quantum information. These studies uncovered a remarkable structure of the $1/N$ fluctuations in the SYK model and established a direct connection to quantum gravity with a black hole in AdS_2 [1,4,5,7,8]. As in the case of a black hole, the scrambling in this system is characterized by a Lyapunov exponent $\lambda_L = 2\pi k_B T / \hbar$ that saturates the universal bound established in Ref. [9]. In light of these results it is natural to ask if there is a broader classification of matter according to how it scrambles information. In particular one may ask if the SYK model can be tuned through a dynamical phase transition to a different state that does not scramble like a black hole.

Here we begin to address these questions by generalizing the SYK model in a way that allows one to drive a quantum phase transition between two low-energy fixed points. The two fixed points entail very different scrambling dynamics, which can be computed exactly in the large- N limit. Specifically we consider the model shown schematically in Fig. 1, with two species of fermions:

$$\mathcal{H} = \mathcal{H}_c + \mathcal{H}_\psi + \mathcal{H}_{c\psi}, \quad (1)$$

where

$$\mathcal{H}_c = \frac{1}{(2N)^{3/2}} \sum_{ijkl} J_{ijkl} c_i^\dagger c_j^\dagger c_k c_l - \mu \sum_i c_i^\dagger c_i, \quad (2a)$$

$$\mathcal{H}_\psi = \frac{1}{M^{1/2}} \sum_{\alpha\beta} t_{\alpha\beta} \psi_\alpha^\dagger \psi_\beta - \mu \sum_\alpha \psi_\alpha^\dagger \psi_\alpha, \quad (2b)$$

$$\mathcal{H}_{c\psi} = \frac{1}{(NM)^{1/4}} \sum_{i\alpha} (V_{i\alpha} c_i^\dagger \psi_\alpha + V_{i\alpha}^* \psi_\alpha^\dagger c_i). \quad (2c)$$

The c fermions, on sites $i = 1, \dots, N$, are described by the SYK model [Eq. (2a)] with random four-fermion coupling J_{ijkl} drawn from a Gaussian distribution with zero mean and variance $\overline{|J_{ijkl}|^2} = J^2$; J_{ijkl} are properly antisymmetrized, i.e., $J_{ijkl} = -J_{jikl} = -J_{ijlk}$ and $J_{ijkl} = J_{klij}$. Here we have adopted a version [8] of the SYK model with complex fermions where one can tune the fermion density by changing the chemical potential μ . The ψ fermions reside on a separate set of “peripheral” sites $\alpha = 1, \dots, M$ connected with each other via hopping $t_{\alpha\beta}$. Finally, there is a coupling $V_{i\alpha}$ between the two species of fermions. Both $t_{\alpha\beta}$ and $V_{i\alpha}$ are complex Gaussian random variables with zero mean and variances $\overline{|t_{\alpha\beta}|^2} = t^2$ and $\overline{|V_{i\alpha}|^2} = V^2$, respectively. The N - and M -dependent prefactors in Eqs. (2) ensure a proper thermodynamic limit for $N, M \rightarrow \infty$ with a fixed ratio $M/N = p$. Evidently, our model reduces to the original SYK model for $p = 0$.

Without the term in Eq. (2c), the model describes two decoupled systems. The SYK Hamiltonian \mathcal{H}_c is solvable in the large- N limit and has an emergent conformal symmetry at low energies [1,5,8]. As mentioned above, the model gives rise to thermalization and many-body quantum chaos with Lyapunov exponent, $\lambda_L = 2\pi T$ ($k_B = 1, \hbar = 1$), that saturates the quantum limit, like a black hole in Einstein gravity [1,9]. The quadratic model alone is also solvable and of course it does not exhibit scrambling.

In this paper we discuss the fate of the coupled system at finite coupling strength V and show that the model leads to an exactly solvable example of a transition between a non-Fermi liquid (NFL) and a Fermi liquid (FL). Since the paper is long and some parts are rather technical, we give an overview of our results here. Our main results are summarized in Fig. 2.

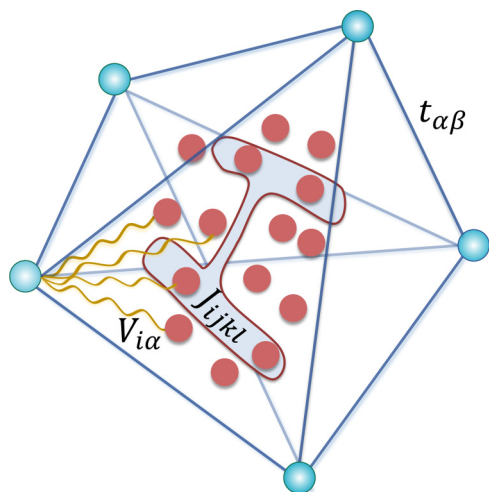


FIG. 1. The generalized SYK model. The SYK sites at the center are coupled through random four-fermion coupling J_{ijkl} . The sites at the periphery are connected to the SYK sites and to each other via random hoppings $V_{i\alpha}$ and $t_{\alpha\beta}$, respectively.

Overview of the results

The low-energy dynamics in the coupled system of SYK fermions coupled to a cloud of noninteracting fermions is crucially determined by the ratio of peripheral sites to SYK sites, $p = M/N$. As shown in Fig. 2, if p is smaller than a critical value $p_c(n)$, with n the fermion density, then the dynamics is still controlled by a strong-coupling SYK-like or NFL fixed point with the universal Lyapunov exponent $\lambda_L = 2\pi T$. On the other hand, for $p > p_c$ the quadratic fermions effectively screen the SYK interactions, leading to a free low-energy fixed point, essentially a FL, characterized at low temperatures by a Lyapunov exponent $\lambda_L = AT^2$ with a nonuniversal prefactor, which is what one may expect if the scrambling occurs via weak inelastic quasiparticle collisions. The two phases are separated by a continuous quantum phase transition at $p = p_c$.

Interestingly, the critical ratio p_c depends only on the fermion density and not on the coupling V or the hopping

strength t . These couplings, however, determine the crossover energy scales below which the two fermion species are effectively coupled and the low-energy fixed-point behavior ensue on the two sides of the transition. The crossover scales, ω_{NFL} and ω_{FL} for the NFL and FL fixed points, respectively, are shown schematically in Fig. 2(b) for the particle-hole symmetric case at half filling, where $p_c = 1$. The surprising insensitivity of the NFL-FL phase boundary to any of the basic energy scales of the model results from the fact that the transition is between two fixed points, each with an emergent low-energy conformal symmetry. As a result the bare couplings drop out from the problem at low energies and the transition is only dictated by entropic factors, as we discuss later.

As depicted in Fig. 2(b), we explicitly show that $\lambda_L = 2\pi T$ in the entire NFL phase for $p < 1$ at half filling. This is not *a priori* obvious as the marginal coupling V to peripheral fermions could have given rise to correction to linear- T coefficient of λ_L . We note that a strong-coupling fixed point itself does not ensure the saturation of the chaos bound [10]. We further extend our calculation of the Lyapunov exponent away from the particle-hole symmetric situation, where there is an additional emergent low-energy U(1) gauge symmetry [8,11], and show that the entire NFL phase in Fig. 2(a) saturates the upper bound on λ_L [9]. To our knowledge, this is the first explicit calculation of λ_L for the SYK model [8] away from half filling. Our results for λ_L imply that, even in the presence of marginal coupling V and/or U(1) gauge symmetry, there is an emergent $SL(2, R)$ symmetry that leads to an effective Schwarzian derivative action at low energy, as studied extensively for the original SYK model [5]. The direct transition from a phase with fast scrambling, which saturates the quantum bound to a slow scrambling phase, suggests there may be a dual picture in terms of a phase transition involving the emergence of a black hole at a critical point of quantum gravity.

The jump of λ_L across the NFL-FL phase boundary might naively suggest a first-order transition, reminiscent of first-order transition in AdS involving the emergence of a black hole at finite temperature [12]. However, we show that two-point functions for the fermions evolve continuously across the transition. The original SYK model has a residual

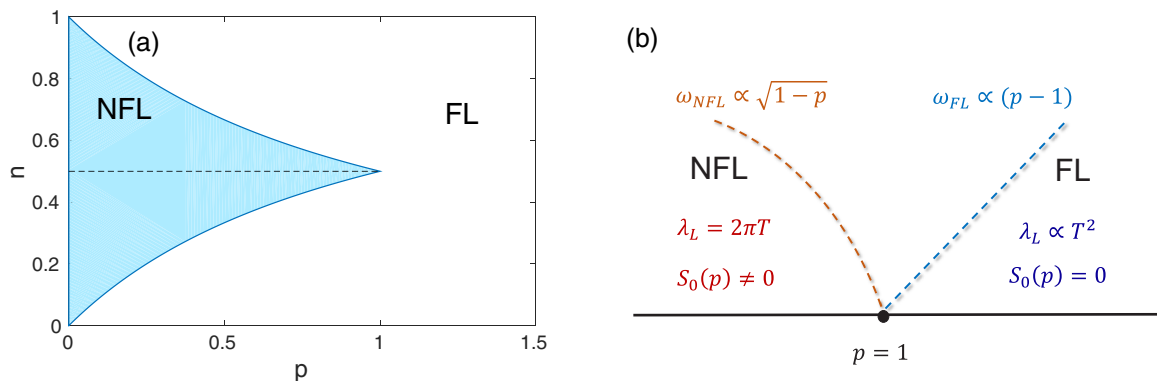


FIG. 2. (a) Phase diagram of the generalized SYK model in the plane of the average fermion filling n and the ratio $p = M/N$. The entire NFL phase saturates the chaos bound, $\lambda_L = 2\pi T$ [9]. The dashed line indicates half filling. (b) Phase diagram at half filling as a function of p . A quantum phase transition separates the NFL and FL at $p = 1$. The latter scrambles with a much slower rate $\propto T^2$. The NFL phase has a residual zero-temperature entropy density S_0 that vanishes continuously at the transition. The crossover scales ω_{NFL} and ω_{FL} for the respective fixed-point behaviors collapse approaching the transition from both sides in the manner shown in the figure panel.

zero-temperature entropy density S_0 [1,8,13]. Using a thermodynamic Maxwell relation and a Luttinger theorem for the NFL fixed point, we show that the residual entropy continuously vanishes at the transition, thereby signaling a fundamental change of the low-energy many-body spectrum across the transition.

We also would like to emphasize that having a transition at a nonzero p in our model is rather unexpected. To demonstrate this fact, we stress the difference between our model and another natural extension of the SYK model. It is tempting to consider a model with both quadratic and quartic couplings of fermions on the same N sites. Since a model with only quadratic coupling between the sites gives rise to a different fixed point than the SYK model, one might naively expect a phase transition separating the two fixed points at some finite ratio of the quadratic-to-quartic couplings. However, in this case the quadratic couplings are relevant and always lead to a free fixed point in the low-energy limit [14]. Hence, in contrast to the model we propose, such a system would not exhibit a quantum critical point (QCP).

Before proceeding we mention that other generalizations of the SYK model were introduced to explore different aspects of the physics [15–17]. For example, Gu and Qi [15] considered a chain of SYK sites coupled through local quartic interactions, which allows one to study the relation between transport coefficients and the butterfly effect in extended systems. Our goal with the model we introduce is different. It is to allow tuning of a quantum critical point separating phases with distinct chaotic behavior.

The rest of the paper is organized as follows. In Sec. II we discuss the coupled self-consistent equations for the Green's functions of the SYK fermions and the peripheral fermions. From the solution we identify the critical point separating the SYK-like phase from the weakly coupled Fermi liquid. In Sec. III we compute the $T = 0$ entropy of the model, showing how it vanishes continuously at the critical point. The weak-coupling phase, unlike the SYK-like phase, has vanishing zero-point entropy. In Sec. IV we turn to compute four-point out-of-time-order (OTO) correlation functions, which encapsulate the scrambling dynamics. The results are discussed and summarized in Sec. V. We also describe the contents of the respective sections in simple terms at the beginning of each section so that readers could in principle skip the technical parts. Some details of the calculations and numerical computations are given in Appendixes A, B, and C and in the Supplemental Material [18].

II. TWO-POINT FUNCTION AND THE QUANTUM CRITICAL POINT

In this section we discuss the Green's functions for the two species of fermions and show how the quantum phase transition as a function p is manifested in the single-particle spectral properties. Here we are interested in the disorder-averaged Green's functions, $G(\tau) = -\langle \mathcal{T}_\tau c(\tau) c^\dagger(0) \rangle$ and $\mathcal{G}(\tau) = -\langle \mathcal{T}_\tau \psi(\tau) \psi^\dagger(0) \rangle$, where τ is the imaginary time and the overbar in $\langle \dots \rangle$ denotes averaging over realizations of $\{J_{ijkl}, t_{\alpha\beta}, V_{i\alpha}\}$. For $N \rightarrow \infty$ the Green's functions can be obtained either diagrammatically or, equivalently, from the

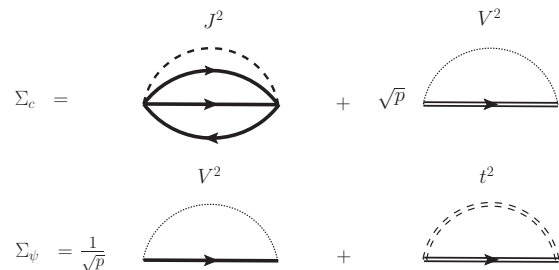


FIG. 3. Self-energy diagrams that contribute at leading order in $1/N$ for a fixed ratio $p = M/N$. The bold lines represent Green's function G of the SYK sites and the double line the Green's function \mathcal{G} for the peripheral sites. The dashed, dotted, and dashed-double lines imply disorder averaging over J_{ijkl} , $V_{i\alpha}$, and $t_{\alpha\beta}$, respectively.

saddle point of an effective action functional obtained via the replica formalism (see Supplemental Material [18]). In either way we obtain the following self-consistent Schwinger-Dyson equations:

$$G^{-1}(i\omega_n) = i\omega_n + \mu - \Sigma_J(i\omega_n) - V^2 \sqrt{p} \mathcal{G}(i\omega_n), \quad (3a)$$

$$\mathcal{G}^{-1}(i\omega_n) = i\omega_n + \mu - \frac{V^2}{\sqrt{p}} G(i\omega_n) - t^2 \mathcal{G}(i\omega_n), \quad (3b)$$

where $\omega_n = (2n + 1)\pi T$ is the fermionic Matsubara frequency and n an integer. The last two terms of each of the equations above correspond to the self-energy diagrams of Fig. 3. Due to the large- N limit and the disorder averaging, only the “rainbow” diagram (Fig. 3), with the bare Green's function lines replaced by the dressed ones, contributes to the interaction correction to the self-energy at leading order in $1/N$ [1,4], i.e.,

$$\Sigma_J(\tau) = -J^2 G^2(\tau) G(-\tau). \quad (3c)$$

As in Refs. [2,8] we define the shifted self-energy $\hat{\Sigma}(i\omega) = \Sigma(i\omega) - \mu$ in order to eliminate the chemical potential from the equations. This shift only affects the behavior at $\tau = 0$ and therefore does not affect Eq. (3c) in the long time limit we are interested in.

Below we show that the coupled self-consistency equations (3) lead to two distinct phases at $T = 0$, tuned by the ratio p . Both phases enjoy an emergent low-energy conformal symmetry, but with distinct scaling dimensions of the fermions. In the NFL phase the SYK fermion spectral function diverges at low frequency as $1/\sqrt{\omega}$, whereas the self-energy is proportional to $\sqrt{\omega}$. For the peripheral fermions the situation is inverted; their spectral function is suppressed at zero bias as $\sqrt{\omega}$. The FL, on the other hand, exhibits a constant spectral function at low energies for both species, whereas the interaction self-energy $\text{Im}\Sigma_J^R(\omega) \sim \omega^2$ is characteristic of a FL. We show that the NFL-FL phase boundary in the n - p plane [Fig. 2(a)] is determined by a Luttinger sum rule for the NFL fixed point and completely impervious to bare energy scales of the model, as discussed earlier. At the end of the section, we verify our analytical results via numerical solution of the self-consistency equations (3).

A. Non-Fermi liquid

The solution for $p < p_c$ is found by first neglecting the terms $i\omega_n$ and $t^2\mathcal{G}(i\omega_n)$ in Eqs. (3), with the expectation that the solution will justify this omission in the low-frequency limit. Without the omitted terms the equations assume the following simple form in imaginary time:

$$\int_0^\beta d\tau_1 G(\tau, \tau_1) [\hat{\Sigma}_J(\tau_1, \tau') + V^2 \sqrt{p} \mathcal{G}(\tau_1, \tau')] = -\delta(\tau - \tau'), \quad (4a)$$

$$\frac{V^2}{\sqrt{p}} \int_0^\beta d\tau_1 \mathcal{G}(\tau, \tau_1) G(\tau_1, \tau') = -\delta(\tau - \tau'). \quad (4b)$$

As in the pure SYK model, these equations along with Eq. (3c) are invariant under arbitrary reparametrization of imaginary time $\tau = f(\sigma)$ with the following scaling of Green's functions and self-energy $\hat{\Sigma}_J$:

$$\tilde{G}(\sigma, \sigma') = [f'(\sigma)f'(\sigma')]^{\Delta_c} G(f(\sigma), f(\sigma')) \frac{g(\sigma')}{g(\sigma)}, \quad (5a)$$

$$\tilde{\mathcal{G}}(\sigma, \sigma') = [f'(\sigma)f'(\sigma')]^{\Delta_\psi} \mathcal{G}(f(\sigma), f(\sigma')) \frac{g(\sigma')}{g(\sigma)}, \quad (5b)$$

$$\tilde{\Sigma}_J(\sigma, \sigma') = [f'(\sigma)f'(\sigma')]^{\Delta_\Sigma} \hat{\Sigma}_J(f(\sigma), f(\sigma')) \frac{g(\sigma')}{g(\sigma)}, \quad (5c)$$

with $f'(\sigma) = \partial f / \partial \sigma$. Here the scaling dimension for SYK fermions is $\Delta_c = 1/4$, the peripheral fermions have the scaling dimension $\Delta_\psi = 3/4$, and $\Delta_\Sigma = 3/4$. The factor $g(\sigma)$, real in imaginary time, is due to an additional emergent U(1) gauge symmetry for the complex fermions as discussed in Ref. [8].

The conformal symmetry of the equations leads to solutions with power-law forms

$$G_R(\omega) = \Lambda \frac{e^{-i(\pi/4+\theta)}}{\sqrt{J\omega}}, \quad (6a)$$

$$\mathcal{G}_R(\omega) = -\frac{\sqrt{p}}{V^2 \Lambda} e^{i(\pi/4+\theta)} \sqrt{J\omega}, \quad (6b)$$

$$\hat{\Sigma}_J^R(\omega) = -\pi^{-1} \Lambda^3 e^{i(\pi/4+\theta)} \cos 2\theta \sqrt{J\omega}, \quad (6c)$$

where we have performed the analytic continuation $i\omega_n \rightarrow \omega + i\eta$ to obtain the retarded Green's functions. The constant Λ , determined by direct substitution of the power-law forms into the conformal self-consistency equations (4), is given by

$$\Lambda = \left(\frac{(1-p)\pi}{\cos 2\theta} \right)^{1/4}. \quad (7)$$

The parameter θ in Eqs. (6) is related to spectral asymmetry and fermion filling through a Luttinger theorem [2,8]. We show in Appendix B that for our model in the NFL fixed point the Luttinger relation takes the form

$$n = \frac{1}{1+p} \left[\left(\frac{1}{2} - \frac{\theta}{\pi} \right) + p \left(\frac{1}{2} + \frac{\theta}{\pi} \right) - (1-p) \frac{\sin 2\theta}{4} \right]. \quad (8)$$

The derivation of this Luttinger relation only uses information about $G(\omega)$, $\mathcal{G}(\omega)$, and $\Sigma_J(\omega)$ for $\omega \rightarrow 0$, known from the conformal limit, and $\omega \rightarrow \infty$, determined by fermion

anticommutation. Hence, the relation does not depend on a cutoff or any other parameter of the model like V , t , or J . To ensure $-\text{Im}G_R(\omega)$, $-\text{Im}\mathcal{G}_R(\omega) > 0$, θ is restricted to the range $[-\pi/4, \pi/4]$, which through the above Luttinger relation determines the range of densities over which the solutions (6) exist, namely,

$$\frac{p}{1+p} \leq n \leq \frac{1}{1+p}. \quad (9)$$

This defines a region on the p - n plane, shown in Fig. 2(a), in which the NFL fixed point exists. We have verified numerically that the above region coincides with the NFL phase (see the Supplemental Material [18]). This implies that the NFL-to-FL transition is only dictated by the constraint on analytical properties of the Green's function instead of the relative strength of the bare coupling constants J , t , and V . The phase θ changes continuously as the density is varied between the lower phase boundary of the NFL, where $\theta = \pi/4$, to the upper boundary, where $\theta = -\pi/4$. $\theta = 0$ corresponds to the particle-hole symmetric line at half filling, where the model of Eq. (1) is essentially equivalent to a model of Majorana fermions discussed in Sec. IV A.

We should further verify that the conformal Green's functions (6) solve the full self-consistency equations (3) at low frequency by directly substituting them in the full equations. This shows that the terms omitted from Eqs. (3) to obtain Eq. (4) become negligible below a cutoff scale ω_{NFL} (see Appendix A). For example, at half filling $\omega_{\text{NFL}} \sim (V^4/t^2J)(\sqrt{1-p/p})$ for $p \rightarrow 1$. Hence, this characteristic frequency scale associated with emergence of conformal symmetry vanishes continuously at a critical point $p_c = 1$ (at half filling). As discussed in the introduction, the location of the critical point depends only on n and p regardless of the coupling strength V between the two species. However, the coupling V does control the frequency scale at which the low-energy fixed point emerges.

A defining feature of the NFL phase of this model, both at half filling and away from half filling, is the singularity at $\omega \rightarrow 0$ in the single-particle spectral functions. The density of states (DOS) of the c fermions behaves as $1/\sqrt{\omega}$, as found in the original model by Sachdev and Ye [2], whereas that of the ψ fermions is suppressed at low frequency as $\sqrt{\omega}$. The latter is similar to the well-known zero-bias suppression due to the combined effect of interaction and disorder [19]. The constant Λ , which determines the strength of the low-frequency singularity, has a singular behavior as the system is tuned toward the phase transition $p \rightarrow p_c$ (or $n \rightarrow n_c$ if the density is used as a tuning parameter).

On the particle-hole symmetric line the strength of the $1/\sqrt{\omega}$ peak in G_R vanishes as $(1-p)^{1/4}$. At the same time the strength of the $\sqrt{\omega}$ singularity in the DOS of the peripheral fermions diverges as $(1-p)^{-1/4}$. The evolution of the low-frequency singularity is quite different when approaching the transition near top and bottom phase boundaries, away from half filling. There, as $\theta \rightarrow \pm\pi/4$, the singularities acquire a strong asymmetry between positive and negative frequencies. For example, near the lower phase boundary we take $\theta = \pi/4 - \delta\theta$ to find the leading behavior of the spectral functions in the small detuning parameter $\delta\theta$. The strength of the $1/\sqrt{\omega}$ singularity in the DOS of the c fermions diverges as $1/\delta\theta^{1/4}$

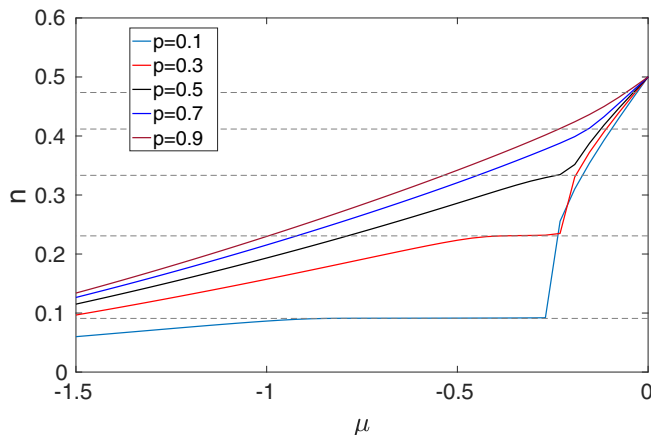


FIG. 4. Fermion density n , below half filling, as a function of the chemical potential μ for $p = 0.1, \dots, 0.9$ (bottom to top curves) at $T = 0.025J$. The dashed lines indicate respective critical densities n_c 's at the lower phase boundary in Fig. 2(a). The plateaus for $p = 0.1, 0.3$ imply the presence of an incompressible state at n_c .

for $\omega > 0$, but vanishes as $\delta\theta^{3/4}$ for $\omega < 0$, whereas the DOS of the peripheral ψ fermions vanishes as $\delta\theta^{1/4}$ for $\omega > 0$ and as $\delta\theta^{5/4}$ for $\omega < 0$. At the same time, the cutoff for the conformal behavior collapses approaching the critical point as $\sim J\delta\theta^{1/2}$ for positive frequencies and as $\sim J\delta\theta^{5/2}$ for negative frequencies.

The vanishing of the spectral functions for $\omega \rightarrow 0^\pm$ on the upper (lower) boundaries may indicate a phase transition into an incompressible state. To assess this possibility we solved the self-consistency equations (3) numerically and obtained the fermion density as a function of the chemical potential at a fixed value of p . The results displayed in Fig. 2(b) indicate a transition to an incompressible state, seen as a plateau in the density. This incompressible state appears as a line in the canonical phase diagram (part of the top and bottom phase boundaries), but it covers a nonvanishing area in the grand-canonical phase diagram μ versus p . For values of p closer to 1, we find a direct transition to a metallic (compressible) Fermi liquid as is also seen in Fig. 4. See the Supplemental Material [18] for more details of the transition away from half filling.

Our discussion so far pertained only to the $T = 0$ Green's functions. Later, for the sake of calculating the out-of-time-order correlation functions, we need the analytic continuation to low nonvanishing temperature. These Green's functions are obtained from the $T = 0$ solutions (6) using the conformal symmetry as shown in Appendix A.

B. Fermi liquid

A different $T = 0$ solution of the self-consistency equations [Eqs. (3)] emerges for $p > p_c(n)$. In this regime we first solve Eqs. (3) by neglecting the interaction self-energy $\Sigma_J(i\omega_n)$ as well as the free $i\omega_n$ terms. In the particle-hole symmetric case $\mu = 0$ ($n = 1/2$), we obtain the following Green's functions:

$$G_R(\omega) = -i \frac{1}{\sqrt{p(p-1)}} \frac{t}{V^2}, \quad (10a)$$

$$\mathcal{G}_R(\omega) = -i \sqrt{\frac{p-1}{p}} \frac{1}{t}, \quad (10b)$$

which correspond to constant DOS. The above is a valid physical solution of the full equations for $p > p_c = 1$ and frequencies much lower than an emergent cutoff scale $\omega_0 \sim (V^2/t)\sqrt{p(p-1)}$ that vanishes at $p = 1$. Also on approaching $p_c = 1$ from above, the low-frequency DOS of the SYK sites diverges as $(p-1)^{-1/2}$ and the DOS of the peripheral sites vanishes as $(p-1)^{1/2}$, continuously merging with the singularities $G(\omega) \sim 1/\sqrt{\omega}$ and $\mathcal{G}(\omega) \sim \sqrt{\omega}$, respectively, on the other side of the transition ($p < p_c$).

To obtain the low-energy free fixed-point solution (10) we have omitted the self-energy $\Sigma_J(i\omega_n)$ from the self-consistency equations (3). We can now feed the solutions back to a calculation of the low-frequency behavior of Σ_J . The result will be valid for $\omega \ll \omega_0$. Our starting point for this calculation is the Fourier-transformed Eq. (3c),

$$\begin{aligned} \Sigma_J(i\omega_n) &= \int_0^\beta d\tau e^{i\omega_n\tau} \Sigma(\tau) \\ &= -\frac{J^2}{\beta^2} \sum_{n_1, n_2} G(i\omega_{n_1}) G(i\omega_{n_2}) G(i\omega_{n_1} + i\omega_{n_2} - i\omega_n). \end{aligned} \quad (11)$$

Carrying out the Matsubara summations and the analytical continuation $i\omega_n \rightarrow \omega + i\eta$ gives (see Supplemental Material [18])

$$\begin{aligned} \text{Im}\Sigma_J^R(\omega > 0) &= -J^2\pi \int_0^{\omega_1+\omega_2 \leq \omega} d\omega_1 d\omega_2 \rho_c(\omega_1) \rho_c(\omega_2) \rho_c(\omega - \omega_1 - \omega_2) \end{aligned} \quad (12)$$

for $T = 0$. In the low-frequency limit, $\omega \ll \omega_0$, the integral can be evaluated using the constant DOS $\rho_c = -(1/\pi)\text{Im}G_R(\omega) = t/(\pi\sqrt{p(p-1)}V^2)$, leading to

$$\text{Im}\Sigma_J^R(\omega) \approx -\frac{J^2 t^3}{2\pi^2 V^6} \frac{1}{[p(p-1)]^{3/2}} \omega^2. \quad (13)$$

Hence, the $T = 0$ quasiparticle decay rate becomes irrelevant and vanishes as ω^2 for $\omega \rightarrow 0$, as expected for a Fermi liquid. At the same time the prefactor of the ω^2 dependence diverges as $(p-1)^{-3/2}$ for $p \rightarrow p_c = 1$, indicating the breakdown of the Fermi liquid at the critical point. We obtain the FL crossover or coherence scale to be $\omega_{\text{FL}} \sim (V^4/Jt^2)(p-1)$ for $p \rightarrow 1$ by estimating the energy scale above which the interaction self-energy effect becomes important, i.e., by comparing $\text{Im}\Sigma_J^R(\omega)$ with the $V^2\sqrt{p}\mathcal{G}(\omega)$ term, which dominates in Eq. (3a) at the FL fixed point (10). ω_{FL} is shown schematically in Fig. 2(b). At the FL fixed point, the saddle-point equations (3) have a trivial emergent conformal symmetry with scaling dimensions $\Delta_c = \Delta_\psi = 1/2$, corresponding to noninteracting fermions.

Hence, the model of Eq. (1) is an example of a solvable model for NFL-FL transition. The transition has some similarity with the overscreening to underscreening transition in the multichannel $\text{SU}(N)$ Kondo impurity model [3]. However, the nature of phases and phase transitions in the multichannel $\text{SU}(N)$ Kondo model is quite different. That model does not exhibit the emergent reparametrization symmetry, which is explicitly broken by the Green's function of the bath. For this reason the overscreened NFL fixed point is not maximally

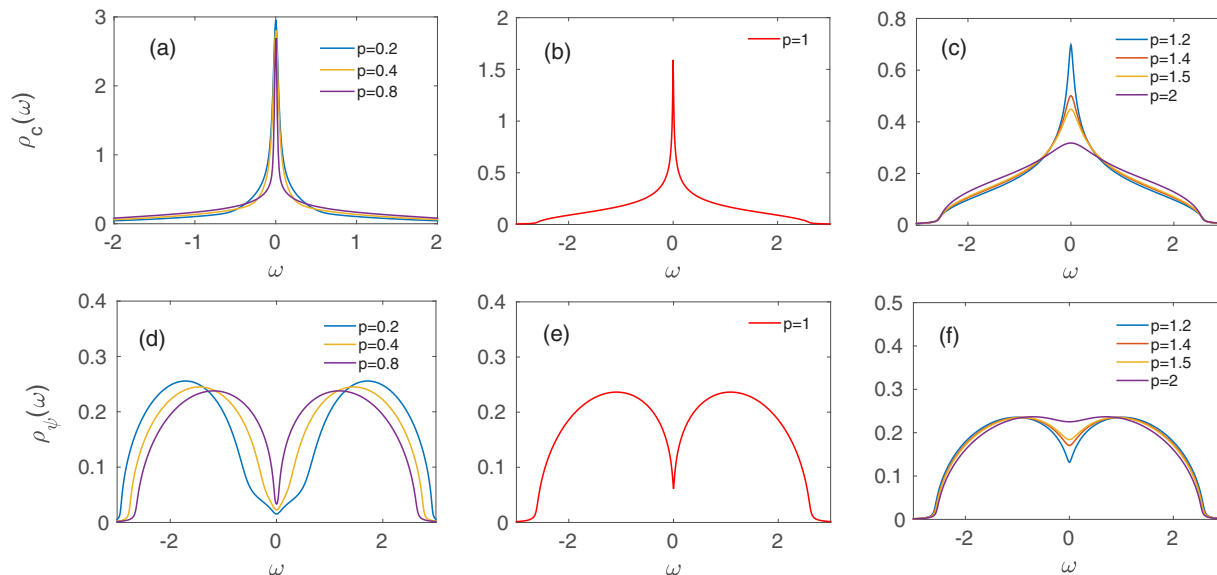


FIG. 5. Numerical results for the single-particle spectral function on the full frequency range taken on (a)–(c) the SYK sites and (d)–(f) the quadratic sites. The spectral functions are computed at $T = 0.025J$ and varying values of p showing how the low-temperature singularities vanish beyond the critical point.

chaotic [20]; hence, it should not have a holographic description in terms of a black hole.

C. Numerical results for spectral function across the QCP

To corroborate the analytical results discussed in the preceding sections, we have solved the self-consistency equations (3) numerically for the retarded Green’s functions $G_R(\omega)$ and $\mathcal{G}_R(\omega)$ over a range of p across the transition. The numerical calculation is performed at finite temperatures.

Here we discuss the results for half filling, $\mu = 0$. The results away from half filling are discussed in the Supplemental Material [18]. In Fig. 5, we show the evolution of spectral functions, $\rho_c(\omega) = -(1/\pi)\text{Im}G_R(\omega)$ and $\rho_\psi(\omega) = -(1/\pi)\text{Im}\mathcal{G}_R(\omega)$, with p for the two species of fermions at $T = 0.025J$ and $t = V = J$. In the NFL phase [Figs. 5(a) and 5(d)], the spectral functions match at low energies with the finite-temperature spectral densities obtained in the conformal limit, showing in particular the $1/\sqrt{\omega}$ and $\sqrt{\omega}$ singularities in $G_R(\omega)$ and $\mathcal{G}_R(\omega)$, respectively. Upon crossing to the FL side of the transition these singularities are rounded off even at $T = 0$. This can be clearly seen deep inside the FL phase for $p = 1.5, 2$ [Figs. 5(c) and 5(f)].

In the next section, we show that the NFL-FL transition also manifests itself in an intriguing way in the evolution of low-temperature entropy.

III. ZERO-TEMPERATURE ENTROPY

The SYK model has an extensive zero-temperature residual entropy [1,8,13] when the thermodynamic limit $N \rightarrow \infty$ is taken before taking the zero-temperature limit. The residual entropy stems from a dense many-body energy spectrum with level spacing $\sim e^{-N}$ [9,13], even near the ground state. In this sense, the low-energy spectrum of the SYK Hamiltonian resembles the spectrum of usual quantum many-body systems at high energies.

In this section, we investigate how the nonzero residual entropy in the pure SYK model evolves as we add an increasing number of peripheral sites (i.e., as a function of p) and in particular how it changes upon crossing the phase transition. The low-energy many-body level spacing in the FL state is expected to vary as $1/N$ and hence residual entropy density is strictly zero for FL. By using a thermodynamic Maxwell relation and the Luttinger sum rule, discussed earlier, we show that the residual entropy of the SYK-like phase vanishes continuously as $(1-p)$ on approaching the transition at half filling. We confirm our analytical result by numerical computation of the low-temperature entropy.

To derive the residual entropy we adopt the scheme outlined in Ref. [8]. The idea is to find the derivative $(\partial S/\partial n)_{T=0}$ as a function of the density n , then perform the integration to the desired density in order to obtain the zero-temperature entropy density $S(T \rightarrow 0) = S_0$. The derivative is found using the Maxwell relation

$$\left(\frac{\partial S}{\partial n}\right)_T = -\left(\frac{\partial \mu}{\partial T}\right)_n. \quad (14)$$

The right-hand side was related in Refs. [8,21] to the spectral asymmetry affected by θ . Specifically, $(\partial \mu/\partial T)_n = -\ln(\tan(\pi/4 + \theta)) + O(T^{2\Delta_c})$. The derivation of this relation is exactly the same here as in the SYK model [8].

Now we can use the Luttinger relation (8), connecting θ to the density, to compute the entropy as an integral over θ :

$$S_0(n) = S_0(n_0) + \int_{n_0}^n dn \ln(\tan(\pi/4 + \theta(n))). \quad (15)$$

Here n_0 refers to a reference density at which the $T = 0$ entropy is known. For example, at $p = 0$, for the pure SYK model, the natural choices are either the empty state, $n_0 = 0$, or the completely filled state, $n_0 = 1$, corresponding to $\theta = \pm\pi/4$, respectively. In these cases we expect $S_0 = 0$ [8]. For general p , this is not as straightforward since the NFL

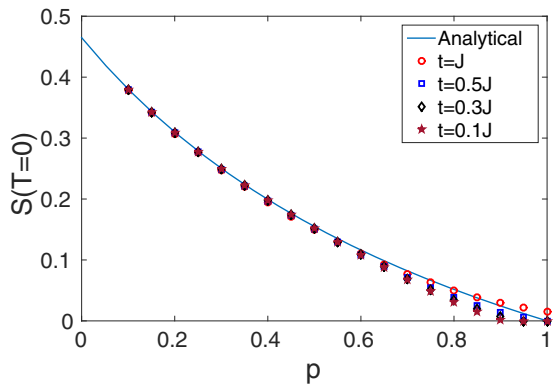


FIG. 6. The zero-temperature limit of the entropy as a function of p . The analytic result using the Luttinger theorem and an assumption $S(T \rightarrow 0) = 0$ at the finite-density phase transition is compared to a direct numerical evaluation of the low-temperature entropy and extrapolations to $T = 0$ for various values of t .

phase only exists up to a lower (upper) critical density $n_c = p/(p+1) > 0$ [$n_c = (p+1)^{-1} < 1$]. However, assuming vanishing of the residual entropy at n_c (upper and lower phase boundaries), that is, $S_0(n_0(\theta = \pm\pi/4)) = 0$, we can take one of the boundaries, e.g., $\theta = \pi/4$, as the reference state to obtain

$$S_0(n(\theta)) = \frac{1-p}{1+p} \int_{\pi/4}^{\theta} d\theta \ln(\cot(\pi/4 + \theta)) \left(\frac{1}{\pi} + \frac{\cos 2\theta}{2} \right). \quad (16)$$

At half filling ($\theta = 0$), we get

$$S_0(n = 1/2) = \frac{1-p}{1+p} S_{\text{SYK}}(T = 0), \quad (17)$$

where $S_{\text{SYK}}(T = 0) \simeq 0.46$ [13,22] is the residual entropy of the SYK model. Hence, the $T = 0$ entropy at half filling vanishes continuously at the QCP as $(1-p)$. At fixed $p < 1$ the entropy vanishes upon approaching the upper and lower phase as $\delta S \sim |n - n_c| \ln(1/|n - n_c|)$.

We corroborate the analytic result for the residual entropy at half filling with a numerical calculation of $S(T)$, extrapolated to $T = 0$ using the linear-in- T behavior of the entropy in the low-temperature conformal limit (see the Supplemental Material [18]). Note that this extrapolation is hindered close to the critical point due to collapse of the cutoff ω_{NFL} beyond which the entropy is no longer linear in T ; hence, the numerical result is not accurate in this regime. The numerically calculated values of the zero-temperature entropy are shown in Fig. 6 and compared to the analytic curve.

Vanishing of the entropy at the critical point suggests a fundamental change of the geometry in the dual gravity picture of the transition, which involves elimination of the black hole. Below we give further evidence to this view from the perspective of the scrambling dynamics. We confirm that the NFL-to-FL critical point marks a transition in the nature of many-body quantum chaos.

IV. OUT-OF-TIME-ORDERED CORRELATIONS: SCRAMBLING

Following Maldacena, Shenker, and Stanford [9], we characterize the scrambling dynamics through a Lyapunov exponent λ_L characterizing the four-point OTO correlation functions. We find $\lambda_L \rightarrow 2\pi T$, saturating the chaos bound [9] in the conformal low-temperature limit, over the entire NFL phase in Fig. 2(a).

The nontrivial (connected) part of the OTO correlation function, e.g., $\langle c_i^\dagger(t)c_j^\dagger(0)c_i(t)c_j(0) \rangle$, appears at order $1/N$ and is expected to grow as $e^{\lambda_L t}$ in the chaos regime. The exact OTO correlation function in the SYK model can be computed in the chaos regime, i.e., $t \ll \lambda_L^{-1} \ln N$ at low temperature [5]. Here we employ a simpler approach, due to Kitaev [1,5], computing the $1/N$ contribution to the OTO correlation function using a self-consistent Bethe-Salpeter-like approximation after formulating the problem on a Keldysh contour with four real-time segments (Appendix C). The self-consistency equations are solved as an eigenvalue problem where the kernel matrix is determined by the saddle-point Green's functions obtained in Sec. II. The eigenfunction with eigenvalue 1 gives the self-consistent solution, which is exponentially growing in the chaotic regime, but it cannot capture the prefactor to the exponential growth.

Below we first obtain λ_L for the NFL at half filling for $T \rightarrow 0$ and show that even in the presence of marginal coupling to peripheral fermions λ_L remains independent of p or the coupling strengths V, t and retains its maximum possible value $2\pi T$. We also calculate λ_L away from half filling in the whole NFL region [Fig. 2(a)] where there is an additional emergent U(1) gauge symmetry [8]. We explicitly show that $\lambda_L = 2\pi T$ for the entire NFL phase as $T \rightarrow 0$. Our results imply that the emergent $SL(2, R)$ symmetry, that leads to the low-energy Schwarzian action in the original SYK model [5], remains intact in the SYK-like phase even in the presence of marginal coupling V and/or additional emergent U(1) gauge symmetry [8,11]. The zero-temperature limit of λ_L changes discontinuously at the critical point from $2\pi T$ in the NFL side to $\lambda_L \propto T^2$ in the FL side, marking the dynamical transition between two distinct chaotic fixed points. At the same point the cutoff scale for the limiting behaviors vanishes, allowing λ_L to be a continuous function of p and T in spite of the apparent discontinuity in the limiting low- T behavior.

A. Majorana fermion model

Before computing the OTO correlations in model (1), we treat a closely related model of Majorana fermions, which admits a much simpler calculation. The generalization to complex fermions at arbitrary filling follows in Sec. IV B. The model consists of two species of Majorana fermions: χ_i in place of the complex fermion c_i on sites $i = 1, \dots, N$ and η_α in place of the fermion ψ_α on sites $\alpha = 1, \dots, M$ (see Fig. 1). Specifically, we consider the following Hamiltonian:

$$\mathcal{H} = \frac{1}{4!} \sum_{ijkl} J_{ijkl} \chi_i \chi_j \chi_k \chi_l + \frac{i}{2!} \sum_{\alpha\beta} t_{\alpha\beta} \eta_\alpha \eta_\beta + i \sum_{i\alpha} V_{i\alpha} \chi_i \eta_\alpha, \quad (18)$$

where J_{ijkl} , $t_{\alpha\beta}$, and $V_{i\alpha}$ are all real; J_{ijkl} and $t_{\alpha\beta}$ are fully antisymmetric and $\langle J_{ijkl}^2 \rangle = J^2 3! / N^3$, $\langle t_{\alpha\beta}^2 \rangle = t^2 / M$, and $\langle V_{i\alpha}^2 \rangle = V^2 / \sqrt{NM}$ with $p = M/N$ as in the complex fermion case. The model leads to the same large- N saddle-point equations as in Eqs. (3) with $\mu = 0$, for the Green's functions $G(\tau) = -\langle \overline{\mathcal{T}_\tau \chi_i(\tau) \chi_j(0)} \rangle$ and $\mathcal{G}(\tau) = -\langle \overline{\mathcal{T}_\tau \eta_\alpha(\tau) \eta_\beta(0)} \rangle$. At $p = 0$, this reduces to the version of the SYK model proposed by Kitaev [1].

The OTO correlations used to diagnose quantum chaos involve four Majorana operators. For example, the OTO correlation on two SYK sites is expected to take the form

$$\overline{\langle \chi_i(t) \chi_j(0) \chi_i(t) \chi_j(0) \rangle} \simeq f_0 - \frac{f_1}{N} e^{\lambda_L t} + O\left(\frac{1}{N^2}\right) \quad (19)$$

and is expected to hold up to some intermediate time scale $t \lesssim t^* \simeq (1/\lambda_L) \ln(N)$, called the scrambling time. This is the time over which the OTO correlation decays to small values and information encoded in local observables is lost to operators encompassing the entire system [9]. Here λ_L is the Lyapunov exponent [23], or scrambling rate, which obeys a universal upper bound $\lambda_L \leq 2\pi T$ [9].

In our model (18), due to the coupling between the SYK fermions χ_i and the peripheral sites η_α , the OTO correlation (19) cannot be found independently of the correlation function describing ‘‘cross scrambling’’ of the SYK sites with the peripheral fermions. Specifically, we compute the following two coupled four-point functions, $F_{\chi\chi\chi\chi} = F_1$ and $F_{\eta\eta\chi\chi} = F_2$:

$$F_1(t_1, t_2) = \frac{1}{N^2} \sum_{ij} \overline{\text{Tr}[y\chi_i(t_1)y\chi_j(0)y\chi_i(t_2)y\chi_j(0)]}, \quad (20a)$$

$$F_2(t_1, t_2) = \frac{1}{NM} \sum_{i\alpha} \overline{\text{Tr}[y\eta_\alpha(t_1)y\chi_i(0)y\eta_\alpha(t_2)y\chi_i(0)]}. \quad (20b)$$

Here we used a modified version of the OTO correlations, in which the four operators are rotated from each other by $1/4$ of the thermal circle, i.e., $y^4 = e^{-\beta\mathcal{H}}/Z$. This modified OTO correlation was introduced in Ref. [9] for computational convenience. The operator y helps to regularize the four-point function in the conformal limit [5,9].

$$\mathcal{K} = \begin{pmatrix} K_{11} & K_{12} \\ K_{21} & K_{22} \end{pmatrix} \simeq \begin{pmatrix} 3J^2 G_R(t_{13})G_R(t_{24})G_{lr}^2(t_{34}) & -V^2\sqrt{p}G_R(t_{13})G_R(t_{24}) \\ -\frac{V^2}{\sqrt{p}}\mathcal{G}_R(t_{13})\mathcal{G}_R(t_{24}) & -t^2\mathcal{G}_R(t_{13})\mathcal{G}_R(t_{24}) \end{pmatrix}. \quad (23)$$

Here $t_{13} = t_1 - t_3$, for example, and $G_{lr}(t) \equiv iG(it + \beta/2)$ is the Wightmann correlator that can be obtained by analytically continuing $G(\tau)$ via $\tau \rightarrow it + \beta/2$ [5].

One can recast Eqs. (22) in the form of an eigenvalue equation, $\mathcal{K}|\mathcal{F}\rangle = k|\mathcal{F}\rangle$, with eigenvalue $k = 1$. Anticipating chaotic dynamics we assume the following ansatz for the function \mathcal{F} :

$$|\mathcal{F}\rangle = \begin{pmatrix} \mathcal{F}_1(t_1, t_2) \\ \mathcal{F}_2(t_1, t_2) \end{pmatrix} = e^{\lambda_L \frac{(t_1+t_2)}{2}} \begin{pmatrix} f_1(t_{12}) \\ f_2(t_{12}) \end{pmatrix}. \quad (24)$$

The Lyapunov exponent $\lambda_L > 0$ can be obtained by computing the eigenvalue k and setting the condition $k(\lambda_L) = 1$ [5].

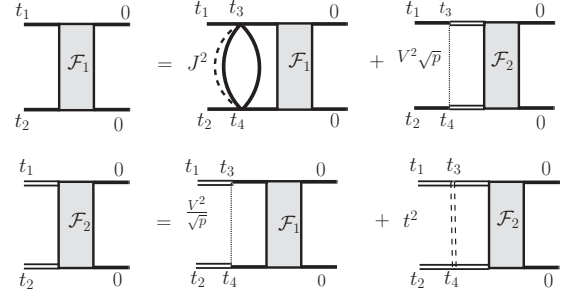


FIG. 7. Diagrammatic illustration of the self-consistency equation [Eq. (22)] for $1/N$ part of the OTO correlation function for Majorana fermions. Solid lines represent the Green's function G , and double lines represent \mathcal{G} . The kernel of Eq. (23) is obtained from the above diagrams for large but intermediate times t_1, t_2 in the chaos regime [1].

Both the four-point functions [Eqs. (20)], $F = F_1, F_2$, can be obtained diagrammatically in the form (see Appendix C)

$$F(t_1, t_2) \simeq F^{(0)}(t_1, t_2) + \frac{1}{N} \mathcal{F}(t_1, t_2) + O\left(\frac{1}{N^2}\right), \quad (21)$$

where $F^{(0)}$ corresponds to $O(1)$ disconnected diagrams from contractions with the dressed propagator obtained from the saddle-point equations (3). The $1/N$ piece \mathcal{F} comes from ladder diagrams (see Appendix C). Following Refs. [1,5], we obtain \mathcal{F} via self-consistent equations represented diagrammatically in Fig. 7,

$$\mathcal{F}_1(t_1, t_2) = \int dt_3 dt_4 [K_{11}(t_1, t_2, t_3, t_4) \mathcal{F}_1(t_3, t_4) + K_{12}(t_1, t_2, t_3, t_4) \mathcal{F}_2(t_3, t_4)], \quad (22a)$$

$$\mathcal{F}_2(t_1, t_2) = \int dt_3 dt_4 [K_{21}(t_1, t_2, t_3, t_4) \mathcal{F}_1(t_3, t_4) + K_{22}(t_1, t_2, t_3, t_4) \mathcal{F}_2(t_3, t_4)], \quad (22b)$$

with the kernel

Using Eq. (24) in Eqs. (22) with the form of the kernel in Eq. (23), we obtain the eigenvalue equation in terms of the Fourier transforms $f_a(\omega) = \int_{-\infty}^{\infty} dt e^{i\omega t} f_a(t)$ ($a = 1, 2$),

$$|G_R(\tilde{\omega})|^2 \left(3J^2 \int_{-\infty}^{\infty} d\omega' g_{lr}(\omega - \omega') f_1(\omega') + V^2 \sqrt{p} f_2(\omega) \right) = k f_1(\omega), \quad (25a)$$

$$|\mathcal{G}_R(\tilde{\omega})|^2 \left(\frac{V^2}{\sqrt{p}} f_1(\omega) + t^2 f_2(\omega) \right) = k f_2(\omega), \quad (25b)$$

where $g_{lr}(\omega) = -\int_{-\infty}^{\infty} (dt/2\pi) G_{lr}^2(t) e^{i\omega t}$ and $\tilde{\omega} = \omega + i\lambda_L/2$.

Lyapunov exponent in the NFL conformal limit. We now solve the above eigenvalue problem analytically in the conformal limit for $T \rightarrow 0$ in the NFL phase. Using the conformal Green's functions of Eqs. (A4) and eliminating f_2 between Eqs. (25a) and (25b), we obtain a single integral equation (see Appendix C),

$$\begin{aligned} \kappa \frac{|\Gamma(\frac{1}{4} + \frac{h}{2} + iu)|^2}{|\Gamma(\frac{3}{4} + \frac{h}{2} + iu)|^2} \int_{-\infty}^{\infty} du' \left| \Gamma\left(\frac{1}{2} + i(u - u')\right) \right|^2 f_1(u') \\ = \left(k - \frac{p}{k}\right) f_1(u), \end{aligned} \quad (26)$$

where $\kappa = (3/4\pi)(1 - p)$, $\lambda_L \equiv 2\pi hT$, and $u = \omega/(2\pi T)$; $\Gamma(x)$ denotes the gamma function. As shown in Appendix C, the following eigenfunction solves the integral equation:

$$f_1(u) = \left| \Gamma\left(\frac{1}{4} + \frac{h}{2} + iu\right) \right|^2, \quad (27)$$

provided that

$$\frac{3(1-p)}{1+2h} = \left(k - \frac{p}{k}\right). \quad (28)$$

The self-consistent solution of Eqs. (22) is obtained by setting $k = 1$ in Eq. (28), leading to $h = 1$, or the Lyapunov exponent

$$\lambda_L = 2\pi T. \quad (29)$$

This implies that the entire NFL phase saturates the chaos bound for $p < 1$ at half filling. This result does not apply at the QCP, since the cutoff for the conformal regime vanishes at $p = 1$ (Appendix A). We leave the low-temperature scrambling dynamics at the QCP for future studies.

In the time domain, Eq. (27) gives

$$f_1(t) \propto [\cosh(\pi t/\beta)]^{-(h+1/2)}, \quad (30)$$

the same as that obtained for the SYK model [5]. The other component f_2 , corresponding to $F_{\eta\chi\chi}$ [Eq. (20b)],

$$f_2(t) \propto \frac{JT}{V^2} \sqrt{\frac{p}{1-p}} \frac{1}{[\cosh(\pi t/\beta)]^{(3/2+h)}}, \quad (31)$$

is suppressed by a factor $\propto T$ relative to f_1 as $T \rightarrow 0$.

B. Lyapunov exponent for arbitrary filling in the NFL phase

We now generalize the calculation of the low-temperature Lyapunov exponent to arbitrary filling in the NFL phase for the complex fermion model (1). In this case, we need to consider the following four coupled out-of-time-order correlation functions:

$$F_1(t_1, t_2) = \frac{1}{N^2} \sum_{ij} \overline{\text{Tr}[yc_i^\dagger(t_1)yc_j^\dagger(0)yc_i(t_2)yc_j(0)]}, \quad (32a)$$

$$F_2(t_1, t_2) = \frac{1}{N^2} \sum_{ij} \overline{\text{Tr}[yc_i(t_1)yc_j^\dagger(0)yc_i^\dagger(t_2)yc_j(0)]}, \quad (32b)$$

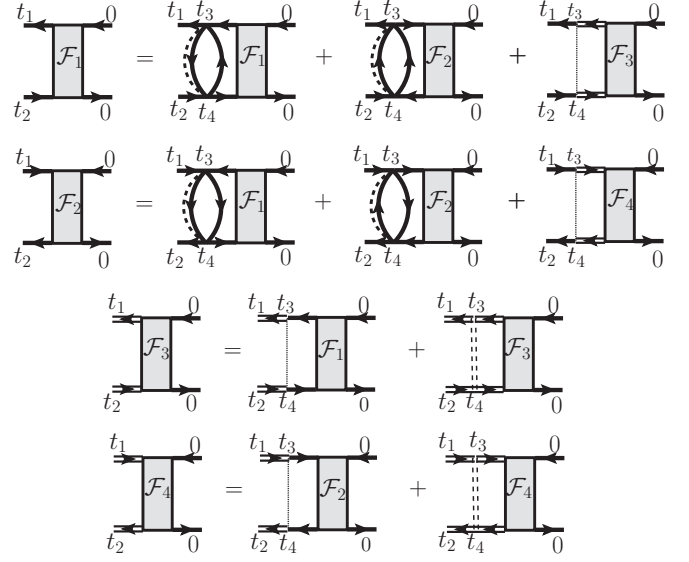


FIG. 8. Diagrammatic representation of the self-consistent approximation for the $1/N$ parts of the out-of-time-order functions for complex fermions.

$$F_3(t_1, t_2) = \frac{1}{NM} \sum_{i\alpha} \overline{\text{Tr}[y\psi_\alpha^\dagger(t_1)yc_i^\dagger(0)y\psi_\alpha(t_2)yc_i(0)]}, \quad (32c)$$

$$F_4(t_1, t_2) = \frac{1}{NM} \sum_{i\alpha} \overline{\text{Tr}[y\psi_\alpha(t_1)yc_i^\dagger(0)y\psi_\alpha^\dagger(t_2)yc_i(0)]}. \quad (32d)$$

As in the case of Majorana fermions, we estimate the $1/N$ part, $|\mathcal{F}\rangle = (\mathcal{F}_1, \mathcal{F}_2, \mathcal{F}_3, \mathcal{F}_4)^T$, of the above four-point functions using the self-consistent approximation shown in Fig. 8. As before, this leads to the eigenvalue equation $\mathcal{K}|\mathcal{F}\rangle = k|\mathcal{F}\rangle$, with the self-consistent solution obtained for the eigenvalue $k = 1$. The nonzero elements of the 4×4 kernel can be approximated in the chaos regime as

$$K_{11} = 2J^2 G_A(t_{31})G_R(t_{24})G_{lr}^+(t_{43})G_{lr}^-(t_{34}),$$

$$K_{12} = -J^2 G_A(t_{31})G_R(t_{24})G_{lr}^+(t_{43})G_{lr}^+(t_{43}),$$

$$K_{21} = -J^2 G_R(t_{13})G_A(t_{42})G_{lr}^-(t_{34})G_{lr}^-(t_{34}),$$

$$K_{22} = 2J^2 G_R(t_{13})G_A(t_{42})G_{lr}^-(t_{34})G_{lr}^+(t_{43}),$$

$$K_{13} = V^2 \sqrt{p} G_A(t_{31})G_R(t_{24}), \quad K_{31} = \frac{V^2}{\sqrt{p}} \mathcal{G}_A(t_{31})\mathcal{G}_R(t_{24}),$$

$$K_{24} = V^2 \sqrt{p} G_R(t_{13})G_A(t_{42}), \quad K_{42} = \frac{V^2}{\sqrt{p}} \mathcal{G}_R(t_{13})\mathcal{G}_A(t_{42}),$$

$$K_{33} = t^2 \mathcal{G}_A(t_{31})\mathcal{G}_R(t_{24}), \quad K_{44} = t^2 \mathcal{G}_R(t_{13})\mathcal{G}_A(t_{42}).$$

There are two Wightmann correlators above, $G_{lr}^+(t) = iG(it + \beta/2)$ and $G_{lr}^-(t) = iG(it - \beta/2)$. The retarded and advanced Green's functions are obtained as $G_R(t) = i\theta(t)[G(it + \eta) - G(it - \eta)]$ and $G_A(t) = i\theta(-t)[G(it - \eta) - G(it + \eta)]$, respectively.

We obtain the Lyapunov exponent for $T \rightarrow 0$ by using the conformal Green's functions of Appendix A in the kernel written above. In this limit, the elements of the kernel are

$$\mathcal{K} = \begin{pmatrix} K_1 e^{i\frac{\alpha}{\beta}(t_{12}-t_{34})} & \frac{1}{2} K_1 \tan\left(\frac{\pi}{4} + \theta\right) e^{i\frac{\alpha}{\beta}(t_{12}+t_{34})} & K_2 e^{i\frac{\alpha}{\beta}(t_{12}-t_{34})} & 0 \\ \frac{1}{2} K_1 \cot\left(\frac{\pi}{4} + \theta\right) e^{-i\frac{\alpha}{\beta}(t_{12}+t_{34})} & K_1 e^{-i\frac{\alpha}{\beta}(t_{12}-t_{34})} & 0 & K_2 e^{-i\frac{\alpha}{\beta}(t_{12}-t_{34})} \\ K_3 e^{i\frac{\alpha}{\beta}(t_{12}-t_{34})} & 0 & K_4 e^{i\frac{\alpha}{\beta}(t_{12}-t_{34})} & 0 \\ 0 & K_3 e^{-i\frac{\alpha}{\beta}(t_{12}-t_{34})} & 0 & K_4 e^{-i\frac{\alpha}{\beta}(t_{12}-t_{34})} \end{pmatrix}, \quad (33)$$

where $\alpha = \ln(\tan(\pi/4 + \theta))$ and

$$K_1(t_1, t_2, t_3, t_4) = \pi(1-p) \tilde{G}_R(t_{13}) \tilde{G}_R(t_{24}) \tilde{G}_{lr}^2(t_{34}), \quad (34a)$$

$$K_2(t_1, t_2, t_3, t_4) = \frac{V^2 \sqrt{p}}{J} \Lambda^2 \tilde{G}_R(t_{13}) \tilde{G}_R(t_{24}), \quad (34b)$$

$$K_3(t_1, t_2, t_3, t_4) = \frac{J \sqrt{p} \pi^2}{4V^2 \Lambda^2} \tilde{G}_R(t_{13}) \tilde{G}_R(t_{24}), \quad (34c)$$

$$K_4(t_1, t_2, t_3, t_4) = \frac{t^2 J p \pi^2}{4V^4 \Lambda^2} \tilde{G}_R(t_{13}) \tilde{G}_R(t_{24}), \quad (34d)$$

with $\tilde{G}_R(t) = \theta(t)/(\beta \sinh(\pi t/\beta))^{1/2}$, $\tilde{G}_{lr}(t) = \theta(t)/(\beta \sinh(\pi t/\beta))^{3/2}$, and $\tilde{G}_{lr}(t) = 1/(\beta \cosh(\pi t/\beta))^{1/2}$.

We transform $\mathcal{K} \rightarrow \tilde{\mathcal{K}}$ by absorbing the exponential phase factors into eigenvector $|\mathcal{F}\rangle$ via the transformation $e^{i(\alpha/\beta)t_{12}}(\mathcal{F}_1, \mathcal{F}_3) = (\tilde{\mathcal{F}}_1, \tilde{\mathcal{F}}_3)$ and $e^{-i(\alpha/\beta)t_{12}}(\mathcal{F}_2, \mathcal{F}_4) = (\tilde{\mathcal{F}}_2, \tilde{\mathcal{F}}_4)$. The eigenvalue equation $\tilde{\mathcal{K}}|\tilde{\mathcal{F}}\rangle = k|\tilde{\mathcal{F}}\rangle$ is solved by the ansatz $|\tilde{\mathcal{F}}\rangle = e^{\lambda_L(t_1+t_2)/2}(af_1(t_{12}), bf_1(t_{12}), f_2(t_{12}), f_3(t_{12}))^T$.

As earlier, we obtain four coupled integral equations,

$$|\tilde{G}_R(\tilde{\omega})|^2 \left[\kappa_1 \int_{-\infty}^{\infty} d\omega' \tilde{g}_{lr}(\omega - \omega') f_1(\omega') + V^2 \sqrt{p} \Lambda^2 f_2(\omega) \right] = k a f_1(\omega), \quad (35a)$$

$$|\tilde{G}_R(\tilde{\omega})|^2 \left[\kappa_2 \int_{-\infty}^{\infty} d\omega' \tilde{g}_{lr}(\omega - \omega') f_1(\omega') + V^2 \sqrt{p} \Lambda^2 f_3(\omega) \right] = k b f_1(\omega), \quad (35b)$$

$$\frac{\sqrt{p} \pi^2}{4V^4 \Lambda^2} |\tilde{G}_R(\tilde{\omega})|^2 [V^2 a f_1(\omega) + t^2 \sqrt{p} f_2(\omega)] = k f_2(\omega), \quad (35c)$$

$$\frac{\sqrt{p} \pi^2}{4V^4 \Lambda^2} |\tilde{G}_R(\tilde{\omega})|^2 [V^2 b f_1(\omega) + t^2 \sqrt{p} f_3(\omega)] = k f_2(\omega), \quad (35d)$$

for the Fourier transforms, $f_a(\omega)$, of $f_a(t)$ ($a = 1, 2, 3$). Here $\tilde{\omega} = \omega + i\lambda_L/2$, $\kappa_1 = \pi(1-p)(a + \frac{1}{2} \tan(\frac{\pi}{4} + \theta)b)$, $\kappa_2 = \pi(1-p)(\frac{1}{2} \cot(\frac{\pi}{4} + \theta)a + b)$, and

$$F_R(z) = \int_{-\infty}^{\infty} dt F_R(t) e^{izt} \quad (\text{Im}z > 0) \\ = \frac{T^{2\Delta-1} \Gamma(\Delta - \frac{iz}{2\pi T})}{\Gamma(2\Delta) \sin(2\pi\Delta) \Gamma(1 - \Delta - \frac{iz}{2\pi T})}, \quad (36a)$$

$$\tilde{g}_{lr}(\omega) = \int_{-\infty}^{\infty} \frac{d\omega'}{2\pi} e^{i\omega t} \tilde{G}_{lr}^2(\omega) = \frac{1}{2\pi^2} \left| \Gamma\left(\frac{1}{2} + \frac{i\omega}{2\pi T}\right) \right|^2, \quad (36b)$$

with $F_R = \tilde{G}_R, \tilde{G}_{lr}$ for $\Delta = 1/4$ and $\Delta = 3/4$, respectively. We can eliminate f_2, f_3 from the first two of Eqs. (35) by using the last two equations. As $T \rightarrow 0$, by defining $h = \lambda_L/2\pi T$ and $u = \omega/2\pi T$, we obtain

$$\frac{\kappa_1}{2\pi^2} \frac{|\Gamma(\frac{1}{4} + \frac{h}{2} + iu)|^2}{|\Gamma(\frac{3}{4} + \frac{h}{2} + iu)|^2} \int_{-\infty}^{\infty} du' \left| \Gamma\left(\frac{1}{2} + i(u-u')\right) \right|^2 f_1(u') \\ = \left(k - \frac{p}{k}\right) a f_1(u),$$

$$\frac{\kappa_2}{2\pi^2} \frac{|\Gamma(\frac{1}{4} + \frac{h}{2} + iu)|^2}{|\Gamma(\frac{3}{4} + \frac{h}{2} + iu)|^2} \int_{-\infty}^{\infty} du' \left| \Gamma\left(\frac{1}{2} + i(u-u')\right) \right|^2 f_1(u') \\ = \left(k - \frac{p}{k}\right) b f_1(u).$$

The above is diagonalized in the frequency space by $f_1(u) = |\Gamma(\frac{1}{4} + \frac{h}{2} + iu)|^2$, as in Eq. (27) for Majorana fermions. As a result we obtain the following eigenvalue equation:

$$\begin{pmatrix} 1 & \frac{1}{2} \tan\left(\frac{\pi}{4} + \theta\right) \\ \frac{1}{2} \cot\left(\frac{\pi}{4} + \theta\right) & 1 \end{pmatrix} \begin{pmatrix} a \\ b \end{pmatrix} = l_k(h) \begin{pmatrix} a \\ b \end{pmatrix}, \quad (37)$$

where $l_k(h) = (k-p/k)(1+2h)/[2(1-p)]$. The eigenvalues are found to be $l_k(h) = 1/2, 3/2$. The self-consistent solution ($k=1$) leads to $h=0, 1$. The latter gives rise to scrambling with the universal Lyapunov exponent $\lambda_L = 2\pi T$. Hence, the entire NFL phase saturates the chaos bound [9].

C. Numerical calculation of the Lyapunov exponent

We have numerically computed λ_L for half filling at finite temperature by solving the eigenvalue equation (25) after discretization over frequency ω . The quantities $G_R(\omega + i\lambda_L/2)$, $\mathcal{G}_R(\omega + i\lambda_L/2)$, and $g_{lr}(\omega)$ appearing in Eq. (25) have been obtained from the numerical solution of the saddle-point equations (3). We solve for the eigenvalues $\{k(\lambda_L)\}$ for a given λ_L and look for λ_L that satisfies $k(\lambda_L) = 1$. We find the eigenvalue $k = 1$ to be nondegenerate.

The numerical result for λ_L as a function of T is shown in Fig. 9(a) over a range of p across QCP. The numerical data are consistent with the ratio $h = \lambda_L \beta / 2\pi$ approaching 1 in the NFL phase within the temperature range that could be accessed. As shown in Fig. 9(b), for $p > 1$, the temperature dependence of λ_L is consistent with a T^2 behavior as expected for a Fermi liquid. This is clearly evident deep in the FL phase for $p \geq 2$.

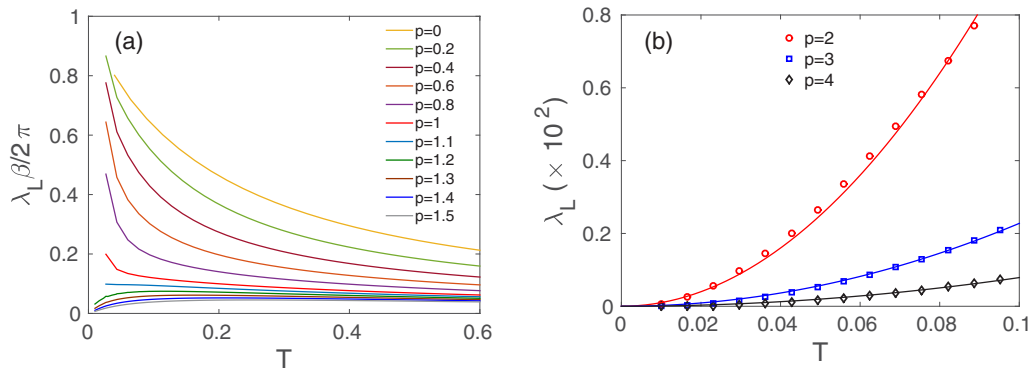


FIG. 9. Numerical results for the temperature dependence of the Lyapunov exponent for various values of p at half filling. (a) $h = \lambda_L \beta / 2\pi$ versus T across the QCP. The difference in the asymptotic low-temperature behaviors of h in the NFL and FL phases is evident. (b) T^2 dependence of the Lyapunov exponent deep in the FL phase at low temperature. The symbols are numerical results and the lines are fits with $\lambda_L \propto T^2$.

V. CONCLUSIONS

In this paper we introduced a solvable model that exemplifies a transition between two classes of many-body quantum chaos. The model is an extension of the SYK model [1,2], with interacting fermions residing on N core sites coupled to a cloud of noninteracting fermions on M peripheral sites. The model is solvable in the scaling limit $N, M \rightarrow \infty$, with $p = M/N$ kept constant. The parameter p tunes the system through a quantum phase transition from the non-Fermi-liquid state established in the pure SYK model to a Fermi-liquid-like phase in which the peripheral fermions screen the interacting core. The residual entropy at $T \rightarrow 0$, which is nonzero in the NFL phase, vanishes continuously upon crossing the critical point. The two phases represent qualitatively different classes of chaotic dynamics embodied in the structure of out-of-time-order correlations. Throughout the NFL phase the Lyapunov exponent, or scrambling rate, characterizing the emergence of chaos, saturates the quantum bound in the low-temperature limit, i.e., $\lambda_L = 2\pi T$. In the Fermi-liquid phase, on the other hand, the scrambling rate is perturbative in the interactions between fermions in the core giving $\lambda_L \propto T^2$ with a nonuniversal prefactor.

The results we have presented for the Lyapunov exponents on either side of the transition are invalidated at the critical point itself. Hence, we postulate that this point represents a new dynamical universality class, which would be an interesting topic for further study. It would also be interesting to understand the holographic interpretation of the transition. The non-Fermi-liquid phase has an established correspondence with a quantum black hole in AdS_2 , which plays the role of the fast scrambler. Therefore, the transition to the free fixed point should correspond to a fundamental change in the geometry that eliminates the black hole. Such correspondence might help to gain insight into the question of black hole evaporation by studying quench across the quantum critical point in our model.

In the model considered here the quantum critical point separates states with fast and slow scrambling. It is natural to ask if further modification of the model is possible that would

bring the chaotic modes to a complete halt while still allowing full analytic control in the large- N limit. Such a solvable model will give us much needed insight into the nature of the many-body localization (MBL) transition. We show elsewhere [24] that a natural generalization of the model discussed here could be used to model a large rare ergodic region within a MBL system. This has implications on the potential instability of MBL in higher dimensions discussed in Ref. [25].

ACKNOWLEDGMENTS

We thank Subir Sachdev, Alexei Kitaev, Yingfei Gu, Xiao-Liang Qi, Ionut-Dragos Potirniche, Snir Gazit, and Karen Micaheli for helpful discussions. This research was supported in part by the ERC synergy grant UQUAM.

APPENDIX A: GREEN'S FUNCTIONS IN THE NFL PHASE

In this Appendix, we obtain the zero- and finite-temperature Green's functions in the conformal limit for the SYK phase. These conformal Green's functions are used to compute the $T = 0$ entropy (Sec. III) and out-of-time-ordered four-point functions (Sec. IV).

At $T = 0$, the imaginary-time functions $F(\tau) = G(\tau), \mathcal{G}(\tau)$ are obtained from the retarded Green's functions in Eqs. (6) via spectral representation

$$\begin{aligned} F(\tau) &= - \int d\omega \frac{\rho(\omega)}{e^{-\beta\omega} + 1} e^{-\omega\tau} \quad (0 < \tau < \beta) \\ &= \int d\omega \frac{\rho(\omega)}{e^{\beta\omega} + 1} e^{-\omega\tau} \quad (-\beta < \tau < 0), \end{aligned} \quad (\text{A1a})$$

where $\rho(\omega) = \rho_c(\omega), \rho_\psi(\omega)$ are the spectral functions for the SYK and peripheral sites, respectively. These lead to

$$\begin{aligned} G(\tau) &= -\Lambda \sin\left(\frac{\pi}{4} + \theta\right) \frac{1}{\sqrt{\pi J \tau}} \quad (0 < \tau) \\ &= \Lambda \cos\left(\frac{\pi}{4} + \theta\right) \frac{1}{\sqrt{-\pi J \tau}} \quad (\tau < 0), \end{aligned} \quad (\text{A2a})$$

$$\begin{aligned} \mathcal{G}(\tau) &= -\frac{\sqrt{p}\pi J^2}{2V^2\Lambda} \sin\left(\frac{\pi}{4} + \theta\right) \frac{1}{(\pi J\tau)^{3/2}} \quad (0 < \tau) \\ &= \frac{\sqrt{p}\pi J^2}{2V^2\Lambda} \cos\left(\frac{\pi}{4} + \theta\right) \frac{1}{(-\pi J\tau)^{3/2}} \quad (\tau < 0). \end{aligned} \quad (\text{A2b})$$

Using Eq. (3c) and the first equation above we can obtain the interaction self-energy,

$$\begin{aligned} \hat{\Sigma}_J(\tau) &= -\frac{J^2\Lambda^3}{2} \cos 2\theta \sin\left(\frac{\pi}{4} + \theta\right) \frac{1}{(\pi J\tau)^{3/2}} \quad (0 < \tau) \\ &= \frac{J^2\Lambda^3}{2} \cos 2\theta \cos\left(\frac{\pi}{4} + \theta\right) \frac{1}{(-\pi J\tau)^{3/2}} \quad (\tau < 0), \end{aligned} \quad (\text{A3})$$

which leads to Eq. (6c). The latter along with Eqs. (6a) and (6b) constitute the self-consistent solution of Eqs. (3) at low energies as can be easily verified.

The conformal symmetry of Eqs. (5) allows one to obtain the finite- T Green's functions from $T = 0$ results [Eqs. (A2)] via conformal transformation, e.g., $\tau = (\beta/\pi) \tan(\pi\sigma/\beta)$ [8], from the infinite line, $-\infty < \tau < \infty$, to the circle $0 < \tau < \beta$. The finite- T Green's functions are

$$\begin{aligned} G(\tau) &= -\Lambda \sin\left(\frac{\pi}{4} + \theta\right) \frac{g(\tau)}{(\beta J \sin(\frac{\pi\tau}{\beta}))^{\frac{1}{2}}} \quad (0 < \tau < \beta) \\ &= \Lambda \cos\left(\frac{\pi}{4} + \theta\right) \frac{g(\tau)}{(\beta J \sin(-\frac{\pi\tau}{\beta}))^{\frac{1}{2}}} \quad (-\beta < \tau < 0), \end{aligned} \quad (\text{A4a})$$

$$\begin{aligned} \mathcal{G}(\tau) &= -\frac{\sqrt{p}\pi J^2}{2V^2\Lambda} \sin\left(\frac{\pi}{4} + \theta\right) \frac{g(\tau)}{(\beta J \sin(\frac{\pi\tau}{\beta}))^{\frac{3}{2}}} \quad (0 < \tau < \beta) \\ &= \frac{\sqrt{p}\pi J^2}{2V^2\Lambda} \cos\left(\frac{\pi}{4} + \theta\right) \frac{g(\tau)}{(\beta J \sin(-\frac{\pi\tau}{\beta}))^{\frac{3}{2}}} \quad (-\beta < \tau < 0). \end{aligned} \quad (\text{A4b})$$

The factor $g(\tau)$ is related to the U(1) gauge factor in Eqs. (5) and can be obtained by imposing the antiperiodic boundary condition $F(\tau + \beta) = -F(\tau)$ on the fermionic Green's functions [8]. This leads to $g(\tau) = e^{-\alpha\tau/\beta}$ with $\alpha = \ln(\tan(\pi/4 + \theta))$, related to the spectral asymmetry.

The above conformal Green's functions can be rewritten in a scaling form ($0 < \tau < \beta$),

$$F(\tau) = -A(\beta J)^{-2\Delta} g\left(\frac{\tau}{\beta}\right), \quad (\text{A5})$$

where $g(x) = e^{-\alpha x}/[\sin(\pi x)]^{2\Delta}$; $\Delta = \Delta_c, \Delta_\psi$, and $A = A_c, A_\psi$ with $A_c = (\Lambda/\sqrt{1 + e^{-2\alpha}})$ and $A_\psi = (\sqrt{p}\pi J^2/(2V^2\Lambda\sqrt{1 + e^{-2\alpha}}))$. From these, one expects the the finite- T

spectral densities to also obey a scaling form

$$\rho(\omega) = \frac{A}{J} \left(\frac{T}{J}\right)^{2\Delta-1} \phi\left(\frac{\omega}{T}\right), \quad (\text{A6})$$

where ϕ is a scaling function. Using these scaling forms [Eqs. (A5) and (A6)] in Eqs. (A1), we obtain $\phi(x)$ following the same procedure as in Ref. [21]. This gives

$$\phi(x) = \frac{2^{2\Delta-1}}{\pi^2} e^{-\alpha/2} \cosh\left(\frac{x}{2}\right) \frac{\Gamma(\Delta + i\frac{x-\alpha}{2\pi})\Gamma(\Delta - i\frac{x-\alpha}{2\pi})}{\Gamma(2\Delta)}. \quad (\text{A7})$$

Here $\Gamma(x)$ is the gamma function. We obtain the conformal Green's functions on the entire complex-frequency (z) plane using Eq. (A6) via the spectral representation

$$F(z) = \int_{-\infty}^{\infty} d\omega \frac{\rho(\omega)}{z - \omega}. \quad (\text{A8})$$

Again following Ref. [21], using the above, we obtain $F(z)$ in a scaling form in the conformal limit for $\Delta < 1/2$; e.g., $F(z) = G_R(z), \mathcal{G}_R(z)$ for $\text{Im}z > 0$ is obtained as

$$F(z) = \frac{A}{J} \left(\frac{T}{J}\right)^{2\Delta-1} \tilde{g}(z/T) \quad (\text{A9a})$$

with the scaling function ($\text{Im}x > 0$)

$$\tilde{g}(x) = -i2^{2\Delta} e^{-\alpha/2} \frac{\cos(\pi\Delta + i\frac{x}{2})}{\Gamma(2\Delta) \sin(2\pi\Delta)} \frac{\Gamma(\Delta - i\frac{x-\alpha}{2\pi})}{\Gamma(1 - \Delta - i\frac{x-\alpha}{2\pi})}. \quad (\text{A9b})$$

The integral in Eq. (A8) has a high-frequency divergence for the conformal spectral function, ρ_ψ , with $\Delta_\psi = 3/4 > 1/2$, for the peripheral sites. However, due to the analytical properties of Γ functions, we can analytically continue the expression in Eqs. (A9) for $\Delta > 1/2$. As a result, Eqs. (A9) also apply for $\mathcal{G}_R(\omega)$ in the conformal limit. We have verified that this ‘‘dimensional regularization’’ of the ultraviolet divergence using the fermion scaling dimension generates quite accurate $\mathcal{G}_R(\omega)$ at low energies when compared with the numerical results, as shown in Fig. 10. We utilize this regularization in Sec. IV to calculate the four-point function in the conformal limit.

Cutoff for the conformal solution in the NFL phase

Here we briefly discuss the frequency cutoff for the conformal solution of Eqs. (6) at half filling. The cutoff is estimated by comparing the terms that are neglected in the conformal limit with those that are retained in Eq. (4), at the NFL fixed point [Eqs. (6)]. To this end, we obtain from Eq. (3a) the condition that $\omega \ll \omega_{c1} + \omega_{c2}$, where

$$\omega_{c1} \simeq \frac{J\Lambda^6}{2\pi^2} = \frac{J}{2\sqrt{\pi}} (1-p)^{3/2}, \quad (\text{A10a})$$

$$\omega_{c2} \simeq \frac{p^2 J}{2\Lambda^2} = \frac{J}{2\sqrt{\pi}} \frac{p^2}{(1-p)^{1/2}}. \quad (\text{A10b})$$

From Eq. (3b), we need to simultaneously satisfy $(V^2/\sqrt{p})G_R(\omega) \gg \omega, t^2\mathcal{G}_R(\omega)$. This leads to the condition

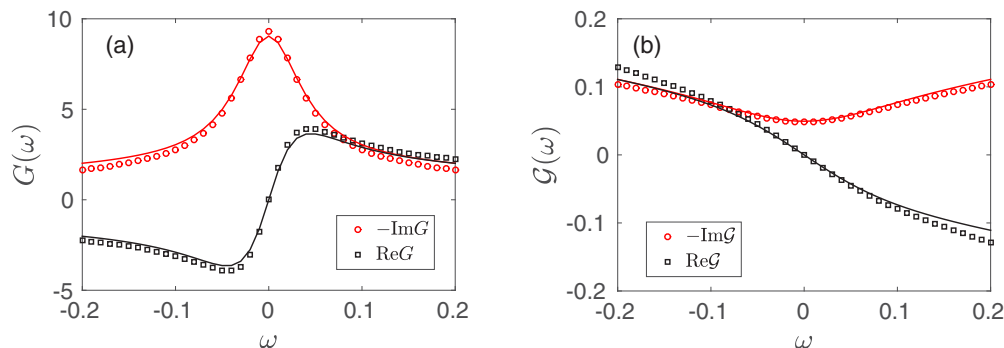


FIG. 10. Comparison between numerically obtained Green's functions (a) G and (b) \mathcal{G} at low frequency with the conformal results of Eqs. (A9) for $p = 0.2$ and $T = 0.025J$.

$\omega \ll (\omega_{c3}, \omega_{c4})$, where

$$\omega_{c3} \simeq \left(\frac{V^4 \Lambda^2}{2pJ} \right)^{1/3} = \left(\frac{\sqrt{\pi} V^4}{2J} \right)^{1/3} \left(\frac{\sqrt{1-p}}{p} \right)^{1/3}, \quad (\text{A10c})$$

$$\omega_{c4} \simeq \frac{V^4 \Lambda^2}{pJt^2} = \frac{\sqrt{\pi} V^4 \sqrt{1-p}}{t^2 J p}. \quad (\text{A10d})$$

The overall cutoff is given by

$$\omega_{\text{NFL}} \approx \min(\omega_{c1} + \omega_{c2}, \omega_{c3}, \omega_{c4}). \quad (\text{A11})$$

For $p \rightarrow 0$, ω_{c1} determines the bandwidth of the conformal behavior, whereas ω_{c4} determines the bandwidth for $p \rightarrow 1$, as shown schematically in Fig. 2(b).

APPENDIX B: LUTTINGER THEOREM IN THE NFL PHASE

In this Appendix we give a proof of the Luttinger theorem [Eq. (8)] used for calculating the zero-temperature entropy in Sec. III. We perform the derivation along the same line of Refs. [21,26].

The total fermion density n at $T = 0$ is given by the sum rule,

$$n = -i \frac{1}{1+p} \int_{-\infty}^{\infty} \frac{d\omega}{2\pi} [G(\omega) + p\mathcal{G}(\omega)] e^{i\omega 0^+}. \quad (\text{B1})$$

$G(\omega)$ and $\mathcal{G}(\omega)$ are the time-ordered Green's functions, e.g., at $T = 0$, $G(\omega) = \theta(\omega)G_R(\omega) + \theta(-\omega)G_A(\omega)$. Here A denotes advanced Green's function.

We rewrite Eq. (B1), by taking the ω derivative of the Dyson equations $G^{-1}(\omega) = \omega + \mu - \Sigma(\omega)$ and $\mathcal{G}^{-1}(\omega) = \omega + \mu - \sigma(\omega)$, as

$$n = \frac{i}{1+p} \left[\mathcal{P} \int_{-\infty}^{\infty} \frac{d\omega}{2\pi} \left(\frac{\partial \ln G}{\partial \omega} + p \frac{\partial \ln \mathcal{G}}{\partial \omega} \right) e^{i\omega 0^+} - \mathcal{P} \int_{-\infty}^{\infty} \frac{d\omega}{2\pi} \left(G \frac{\partial \Sigma_G}{\partial \omega} + p \mathcal{G} \frac{\partial \Sigma_{\mathcal{G}}}{\partial \omega} \right) e^{i\omega 0^+} \right], \quad (\text{B2})$$

where

$$\Sigma(\omega) = \Sigma_J(\omega) + V^2 \sqrt{p} \mathcal{G}(\omega), \quad (\text{B3a})$$

$$\sigma(\omega) = \frac{V^2}{\sqrt{p}} G(\omega) + t^2 \mathcal{G}(\omega). \quad (\text{B3b})$$

Following a procedure similar to that in Ref. [26], we evaluate each of the terms in Eq. (B2) separately. From the first term in Eq. (B2) we get

$$\mathcal{P} \int_{-\infty}^{\infty} \frac{d\omega}{2\pi} \frac{\partial \ln G}{\partial \omega} e^{i\omega 0^+} = \mathcal{P} \int_{-\infty}^{\infty} \frac{d\omega}{2\pi} \frac{\partial \ln G_R}{\partial \omega} e^{i\omega 0^+} + \int_{-\infty}^0 \frac{d\omega}{2\pi} \frac{\partial}{\partial \omega} \ln \left(\frac{G_A}{G_R} \right) e^{i\omega 0^+}, \quad (\text{B4})$$

and similarly for $\mathcal{G}(\omega)$. The second integral above can be evaluated using $G_{R(A)}(\omega) = |G_R(\omega)| e^{\pm i \arg G_R(\omega)}$, leading to

$$\int_{-\infty}^0 \frac{d\omega}{2\pi} \frac{\partial}{\partial \omega} \ln \left(\frac{G_A}{G_R} \right) e^{i\omega 0^+} = -i \left[\frac{1}{4} - \frac{\theta}{\pi} \right], \quad (\text{B5})$$

since $\arg G_R(0^-) = -(3\pi/4 + \theta)$ from Eq. (6) and $\arg G_R(-\infty) = -\pi$. Similarly

$$\int_{-\infty}^0 \frac{d\omega}{2\pi} \frac{\partial}{\partial \omega} \ln \left(\frac{\mathcal{G}_A}{\mathcal{G}_R} \right) e^{i\omega 0^+} = -i \left[\frac{3}{4} + \frac{\theta}{\pi} \right], \quad (\text{B6})$$

using $\arg \mathcal{G}_R(0^-) = -\pi/4 + \theta$ from Eq. (6).

The first integral in Eq. (B4) is evaluated using the conformal solution [Eq. (6)] as

$$\mathcal{P} \int_{-\infty}^{\infty} \frac{d\omega}{2\pi} \frac{\partial \ln G_R}{\partial \omega} e^{i\omega 0^+} = -\frac{i}{4}, \quad (\text{B7})$$

via the deformation of the contour of integration to the upper-half plane since $G_R(\omega)$ is analytic there. Analogously,

$$\mathcal{P} \int_{-\infty}^{\infty} \frac{d\omega}{2\pi} \frac{\partial \ln \mathcal{G}_R}{\partial \omega} e^{i\omega 0^+} = \frac{i}{4}. \quad (\text{B8})$$

Using Eqs. (B5)–(B8) we finally obtain

$$\begin{aligned} & \frac{i}{1+p} \mathcal{P} \int_{-\infty}^{\infty} \frac{d\omega}{2\pi} \left(\frac{\partial \ln G}{\partial \omega} + p \frac{\partial \ln \mathcal{G}}{\partial \omega} \right) e^{i\omega 0^+} \\ &= \frac{1}{1+p} \left[\left(\frac{1}{2} - \frac{\theta}{\pi} \right) + p \left(\frac{1}{2} + \frac{\theta}{\pi} \right) \right]. \end{aligned} \quad (\text{B9})$$

The second term in Eq. (B2) is rewritten using Eqs. (B3a) and (B3b) as

$$\begin{aligned} \mathcal{P} \int_{-\infty}^{\infty} \frac{d\omega}{2\pi} \left(G \frac{\partial \Sigma}{\partial \omega} + p \mathcal{G} \frac{\partial \sigma}{\partial \omega} \right) e^{i\omega 0^+} \\ = \mathcal{P} \int_{-\infty}^{\infty} \frac{d\omega}{2\pi} \left[G \frac{\partial \Sigma_J}{\partial \omega} + V^2 \sqrt{p} \frac{\partial (G\mathcal{G})}{\partial \omega} + \frac{t^2}{2} p \frac{\partial (\mathcal{G}^2)}{\partial \omega} \right]. \end{aligned} \quad (\text{B10})$$

The last two terms give only boundary terms that vanish. Hence, we are left with only the first term inside the bracket above. The evaluation of this term is rather cumbersome and was done by Georges *et al.* [26]. The calculation again only uses the information about the Green's function as $\omega \rightarrow 0$ and hence does not depend on the cutoff. Using the result from Ref. [26] we get

$$i\mathcal{P} \int_{-\infty}^{\infty} \frac{d\omega}{2\pi} G \frac{\partial \Sigma_J}{\partial \omega} = (1-p) \frac{\sin 2\theta}{4}. \quad (\text{B11})$$

The only difference in our case from Ref. [26] is the initial prefactor $(1-p)$, which is crucial. Finally, combining the above with Eq. (B9), we obtain the Luttinger theorem of Eq. (8) in Sec. III.

APPENDIX C: OUT-OF-TIME-ORDERED CORRELATIONS

The out-of-time-ordered correlations of Eqs. (20) can be computed by formulating the problem on a Keldysh contour with four real-time segments, $\gamma = 1, 2, 3, 4$, two forward and two backward in time [27–29]. Each of the consecutive segments is separated by a quarter of the thermal cycle [5] (see Fig. 11). The out-of-time-ordered functions become contour ordered in the Keldysh formalism, e.g., $F_1(t_1, t_2) = (1/N^2) \sum_{ij} \langle \chi_i^4(t_1) \chi_j^3(0) \chi_i^2(t_2) \chi_j^1(0) \rangle$, where $\chi_i^\gamma(t)$ denotes Grassmann variable on the branch γ . In principle, these out-of-time-ordered functions are coupled with four-point functions having various other time orderings, e.g., $\langle \chi_i^4(t_1) \chi_j^3(0) \chi_i^3(t_2) \chi_j^1(0) \rangle$. However, since the out-of-time-ordered functions decay in parametrically longer times $t \lesssim (1/\lambda_L) \ln N$ than the other four-point functions, the former effectively gets decoupled from the latter in the chaos regime.

The first few terms in diagrammatic expansions for $F_1(t_1, t_2)$ and $F_2(t_1, t_2)$ until $O(1/N)$ are shown in Fig. 12. Due to disorder averaging over $\{J_{ijkl}, t_{\alpha\beta}, V_{i\alpha}\}$, only the ladder

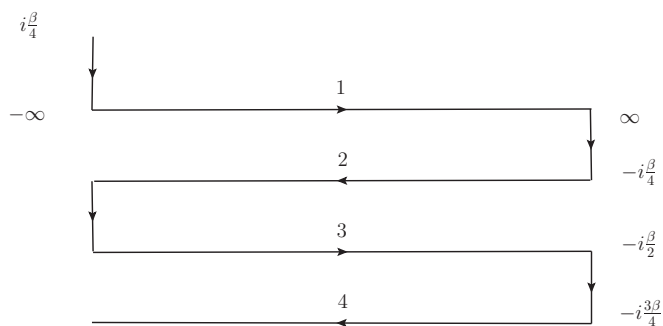


FIG. 11. Keldysh contour with a pair of real-time folds. Subsequent horizontal segments are separated by a quarter of the thermal cycle.

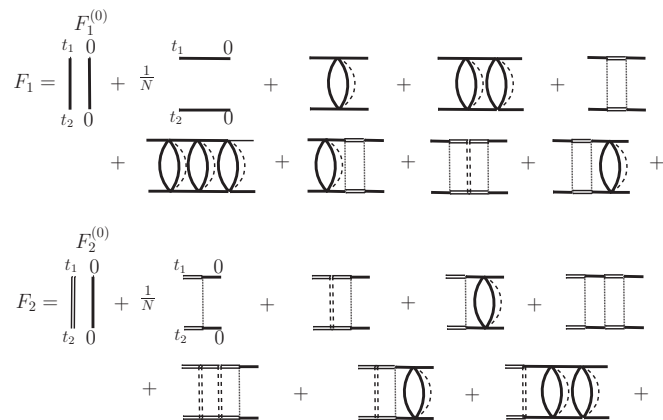


FIG. 12. A few lowest-order diagrams corresponding to OTO correlation functions of Eqs. (20). $F_1^{(0)}$ and $F_2^{(0)}$ denote the disconnected diagrams at $O(1)$. Only ladder diagrams contribute to the $1/N$ pieces \mathcal{F}_1 and \mathcal{F}_2 , which are obtained via the self-consistent approximation of Fig. 7.

diagrams contribute to the $1/N$ pieces $\mathcal{F}_1(t_1, t_2)$ and $\mathcal{F}_2(t_1, t_2)$. These can be obtained in the chaos regime via Eqs. (22), as discussed in Sec. IV.

The retarded functions $F_R(\omega + i\lambda_L/2)$ ($F_R = G_R, \mathcal{G}_R$) and the Wightman correlator $G_{lr}(\omega)$, appearing in Eqs. (25), are obtained from the spectral representations

$$F_R\left(i\frac{\lambda_L}{2} + \omega\right) = \int_{-\infty}^{\infty} d\omega' \frac{\rho(\omega')}{\omega + i\frac{\lambda_L}{2} - \omega'}, \quad (\text{C1a})$$

$$G_{lr}(\omega) = -i\pi \frac{\rho_c(\omega)}{2 \cosh(\beta\omega/2)}, \quad (\text{C1b})$$

with $\rho(\omega) = \rho_c(\omega), \rho_\psi(\omega)$. The above leads to

$$\begin{aligned} g_{lr}(\omega) &= - \int_{-\infty}^{\infty} \frac{dt}{2\pi} G_{lr}^2(t) e^{i\omega t} \\ &= \frac{1}{4} \int_{-\infty}^{\infty} d\omega' \frac{\rho(\omega') \rho(\omega - \omega')}{\cosh(\beta\omega'/2) \cosh(\beta(\omega - \omega')/2)}. \end{aligned} \quad (\text{C1c})$$

Due to particle-hole symmetry, $G_R(\omega + i\lambda_L/2)G_R(-\omega + i\lambda_L/2) = -|G_R(\omega + i\lambda_L/2)|^2$. This identity was used in Eqs. (25).

In the numerical solution of Eqs. (25), discussed in Sec. IV, we use the spectral representations of Eqs. (C1).

1. Solution of Eqs. (25) in the conformal limit

In the conformal limit, we use the Green's functions of Eqs. (A9) to obtain

$$G_R\left(i\frac{\lambda_L}{2} + i\omega\right) = -i \frac{\Lambda}{\sqrt{2\pi J T}} \frac{\Gamma\left(\frac{1}{4} + \frac{h}{2} - iu\right)}{\Gamma\left(\frac{3}{4} + \frac{h}{2} - iu\right)}, \quad (\text{C2a})$$

$$\mathcal{G}_R\left(i\frac{\lambda_L}{2} + i\omega\right) = i \frac{\sqrt{2p\pi J T}}{V^2 \Lambda} \frac{\Gamma\left(\frac{3}{4} + \frac{h}{2} - iu\right)}{\Gamma\left(\frac{1}{4} + \frac{h}{2} - iu\right)}, \quad (\text{C2b})$$

with $\lambda_L \equiv 2\pi h T$ and $u \equiv \omega/(2\pi T)$. From Eq. (A4), the Wightman correlator is $G_{lr}(t) = iG(it + \beta/2) = -i(\Lambda/\sqrt{2})$

$(\beta J \cosh(\pi t/\beta))^{-1/2}$, leading to

$$g_{lr}(\omega) = \frac{\Lambda^2}{4\pi^2 J} |\Gamma(1/2 + iu)|^2. \quad (\text{C2c})$$

Using Eqs. (C2) in Eqs. (25), we get the eigenvalue equation (26) for $T \rightarrow 0$. The component $f_2(u)$ is obtained from $f_1(u)$,

$$f_2(u) = \frac{2\sqrt{\pi}JT}{V^2k} \sqrt{\frac{p}{1-p}} \frac{|\Gamma(\frac{3}{4} + \frac{h}{2} + iu)|^2}{|\Gamma(\frac{1}{4} + \frac{h}{2} + iu)|^2} f_1(u). \quad (\text{C3})$$

Using the form of $f_1(u)$ [Eq. (27)] above we get Eq. (31) in Sec. IV.

To verify that $f_1(u)$ in Eq. (27) is a solution of Eq. (26), we use the identity [30]

$$\begin{aligned} & \int_{-\infty}^{\infty} du' \left| \Gamma\left(\frac{1}{2} + i(u - u')\right) \right|^2 \left| \Gamma\left(\frac{1}{4} + \frac{h}{2} + iu'\right) \right|^2 \\ &= 2\pi \frac{\Gamma(\frac{1}{2} + h)}{\Gamma(\frac{3}{2} + h)} \left| \Gamma\left(\frac{3}{4} + \frac{h}{2} + iu\right) \right|^2. \end{aligned} \quad (\text{C4})$$

2. The functions $F_{\chi\chi\eta\eta}(t_1, t_2)$ and $F_{\eta\eta\eta\eta}(t_1, t_2)$

We can also define two other out-of-time-ordered functions, $F_3 = F_{\chi\chi\eta\eta}$ and $F_4 = F_{\eta\eta\eta\eta}$, as

$$F_3(t_1, t_2) = \frac{1}{NM} \sum_{i\alpha} \overline{\text{Tr}[y\chi_i(t_1)y\eta_\alpha(0)y\chi_i(t_2)y\eta_\alpha(0)]}, \quad (\text{C5a})$$

$$F_4(t_1, t_2) = \frac{1}{M^2} \sum_{\alpha\beta} \overline{\text{Tr}[y\eta_\alpha(t_1)y\eta_\beta(0)y\eta_\alpha(t_2)y\eta_\beta(0)]}, \quad (\text{C5b})$$

denoted by F_3 and F_4 , respectively. The $1/N$ pieces of these functions, \mathcal{F}_3 and \mathcal{F}_4 , follow exactly same equation as in Eq. (22) with \mathcal{F}_1 replaced by \mathcal{F}_3 and \mathcal{F}_2 by \mathcal{F}_4 . Hence, \mathcal{F}_3 and \mathcal{F}_4 have the same solutions as \mathcal{F}_1 and \mathcal{F}_2 , respectively, discussed in Sec. IV. However, there is a suppression of F_3 by a factor $(JT/V^2)\sqrt{p/(1-p)}$ compared to F_1 . This can be seen by evaluating the disconnected diagrams (Fig. 12) contributing to F_1 and F_3 .

-
- [1] A. Kitaev, A simple model of quantum holography (unpublished).
 - [2] Subir Sachdev and Jinwu Ye, Gapless Spin-Fluid Ground State in a Random Quantum Heisenberg Magnet, *Phys. Rev. Lett.* **70**, 3339 (1993).
 - [3] Olivier Parcollet and Antoine Georges, Transition from Overscreening to Underscreening in the Multichannel Kondo Model: Exact Solution at Large N , *Phys. Rev. Lett.* **79**, 4665 (1997).
 - [4] Joseph Polchinski and Vladimir Rosenhaus, The spectrum in the Sachdev-Ye-Kitaev model, *J. High Energy Phys.* **04** (2016) 001.
 - [5] Juan Maldacena and Douglas Stanford, Comments on the Sachdev-Ye-Kitaev model, *Phys. Rev. D* **94**, 106002 (2016).
 - [6] Dmitry Bagrets, Alexander Altland, and Alex Kamenev, Sachdev-Ye-Kitaev model as Liouville quantum mechanics, *Nucl. Phys. B* **911**, 191 (2016).
 - [7] Subir Sachdev, Holographic Metals and the Fractionalized Fermi Liquid, *Phys. Rev. Lett.* **105**, 151602 (2010).
 - [8] Subir Sachdev, Bekenstein-Hawking Entropy and Strange Metals, *Phys. Rev. X* **5**, 041025 (2015).
 - [9] Juan Maldacena, Stephen H. Shenker, and Douglas Stanford, A bound on chaos, *J. High Energy Phys.* **08** (2016) 106.
 - [10] A. A. Patel and S. Sachdev, Quantum chaos on a critical Fermi surface, *Proc. Natl. Acad. Sci. USA* **114**, 1844 (2017).
 - [11] R. A. Davison, W. Fu, A. Georges, Y. Gu, K. Jensen, and S. Sachdev, Thermoelectric transport in disordered metals without quasiparticles: The SYK models and holography, [arXiv:1612.00849](https://arxiv.org/abs/1612.00849).
 - [12] E. Witten, Anti-de Sitter space, thermal phase transition, and confinement in gauge theories, *Adv. Theor. Math. Phys.* **2**, 505 (1998).
 - [13] Wenbo Fu and Subir Sachdev, Numerical study of fermion and boson models with infinite-range random interactions, *Phys. Rev. B* **94**, 035135 (2016).
 - [14] Olivier Parcollet and Antoine Georges, Non-Fermi-liquid regime of a doped Mott insulator, *Phys. Rev. B* **59**, 5341 (1999).
 - [15] Y. Gu, X.-L. Qi, and D. Stanford, Local criticality, diffusion and chaos in generalized Sachdev-Ye-Kitaev models, [arXiv:1609.07832](https://arxiv.org/abs/1609.07832).
 - [16] M. Berkooz, P. Narayan, M. Rozali, and J. Simón, Higher dimensional generalizations of the SYK model, *J. High Energy Phys.* **01** (2017) 138.
 - [17] D. J. Gross and V. Rosenhaus, A generalization of Sachdev-Ye-Kitaev, *J. High Energy Phys.* **02** (2017) 093.
 - [18] See Supplemental Material at <http://link.aps.org/supplemental/10.1103/PhysRevB.95.134302> for the details of the calculations of thermodynamic quantities, numerical solutions of saddle-point equations, and the results for spectral function away from half filling.
 - [19] B. L. Altshuler and A. G. Aronov, in *Electron-Electron Interactions in Disordered Systems*, edited by A. J. Efros and M. Pollak (Elsevier, Amsterdam, 1985).
 - [20] S. Gazit, I.-D. Potirniche, S. Banerjee, and E. Altman (unpublished).
 - [21] Olivier Parcollet, Antoine Georges, Gabriel Kotliar, and Anirvan Sengupta, Overscreened multi-channel $SU(N)$ Kondo model: Large- N solution and conformal field theory, *Phys. Rev. B* **58**, 3794 (1998).
 - [22] A. Georges, O. Parcollet, and S. Sachdev, Mean Field Theory of a Quantum Heisenberg Spin Glass, *Phys. Rev. Lett.* **85**, 840 (2000).
 - [23] A. I. Larkin and Yu. N. Ovchinnikov, Quasiclassical method in the theory of superconductivity, *JETP* **28**, 1200 (1969).
 - [24] I.-D. Potirniche, S. Banerjee, and E. Altman (unpublished).
 - [25] W. De Roeck and F. Huveneers, Stability and instability towards delocalization in MBL systems, [arXiv:1608.01815](https://arxiv.org/abs/1608.01815).
 - [26] A. Georges, O. Parcollet, and S. Sachdev, Quantum fluctuations of a nearly critical Heisenberg spin glass, *Phys. Rev. B* **63**, 134406 (2001).

- [27] Douglas Stanford, Many-body chaos at weak coupling, *J. High Energy Phys.* **10** (2016) 009.
- [28] I. L. Aleiner, L. Faoro, and L. B. Ioffe, Microscopic model of quantum butterfly effect: Out-of-time-order correlators and traveling combustion waves, *Ann. Phys.* **375**, 378 (2016).
- [29] F. M. Haehl, R. Loganayagam, and M. Rangamani, Schwinger-Keldysh formalism I: BRST symmetries and superspace, [arXiv:1610.01940](https://arxiv.org/abs/1610.01940).
- [30] I. S. Gradshteyn and I. M. Ryzhik, *Table of Integrals, Series, and Products*, 7th ed., edited by A. Jeffrey and D. Zwillinger (Academic Press, Amsterdam, 2007).